










RESEARCH ARTICLE | SEPTEMBER 05 2023

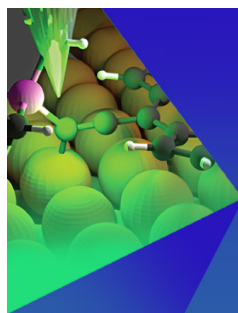
Efficiency of charge transfer in changing the dissociation dynamics of OD⁺ transients formed after the photo-fragmentation of D₂O

W. Iskandar ; T. N. Rescigno ; A. E. Orel ; T. Severt ; K. A. Larsen ; Z. L. Streeter; B. Jochim ; B. Griffin; D. Call ; V. Davis ; C. W. McCurdy ; R. R. Lucchese ; J. B. Williams; I. Ben-Itzhak ; D. S. Slaughter ; Th. Weber  



J. Chem. Phys. 159, 094301 (2023)

<https://doi.org/10.1063/5.0159300>



Chemical Physics Reviews

Special Topics
Open for Submissions

[Learn more](#)



Efficiency of charge transfer in changing the dissociation dynamics of OD⁺ transients formed after the photo-fragmentation of D₂O

Cite as: J. Chem. Phys. 159, 094301 (2023); doi: 10.1063/5.0159300

Submitted: 22 May 2023 • Accepted: 7 August 2023 •

Published Online: 5 September 2023



View Online



Export Citation



CrossMark

W. Iskandar,¹ T. N. Rescigno,¹ A. E. Orel,² T. Severt,³ K. A. Larsen,^{1,4} Z. L. Streeter,^{1,5} B. Jochim,³ B. Griffin,^{1,6} D. Call,⁶ V. Davis,⁶ C. W. McCurdy,^{1,5} R. R. Lucchese,¹ J. B. Williams,⁶ I. Ben-Itzhak,³ D. S. Slaughter,¹ and Th. Weber^{1,a)}

AFFILIATIONS

¹Chemical Sciences Division, Lawrence Berkeley National Laboratory, Berkeley, California 94720, USA

²Chemical Engineering, University of California, Davis, California 95616, USA

³J.R. Macdonald Laboratory, Department of Physics, Kansas State University, Manhattan, Kansas 66506, USA

⁴Graduate Group in Applied Science and Technology, University of California, Berkeley, California 94720, USA

⁵Department of Chemistry, University of California, Davis, California 95616, USA

⁶Department of Physics, University of Nevada, Reno, Nevada 89557, USA

^{a)}Author to whom correspondence should be addressed: tweber@lbl.gov

ABSTRACT

We present an investigation of the relaxation dynamics of deuterated water molecules after direct photo-double ionization at 61 eV. We focus on the very rare D⁺ + O⁺ + D reaction channel in which the sequential fragmentation mechanisms were found to dominate the dynamics. Aided by theory, the state-selective formation and breakup of the transient OD⁺ (a¹Δ, b¹Σ⁺) is traced, and the most likely dissociation path—OD⁺: a¹Δ or b¹Σ⁺ → A³Π → X³Σ⁻ → B³Σ⁻—involving a combination of spin-orbit and non-adiabatic charge transfer transitions is determined. The multi-step transition probability of this complex transition sequence in the intermediate fragment ion is directly evaluated as a function of the energy of the transient OD⁺ above its lowest dissociation limit from the measured ratio of the D⁺ + O⁺ + D and competing D⁺ + D⁺ + O sequential fragmentation channels, which are measured simultaneously. Our coupled-channel time-dependent dynamics calculations reproduce the general trends of these multi-state relative transition rates toward the three-body fragmentation channels.

Published under an exclusive license by AIP Publishing. <https://doi.org/10.1063/5.0159300>

I. INTRODUCTION

The concept of reaction coordinates is elemental in chemistry as it describes the evolution from reactants to products with various intermediates and transition states in between. Transition states and their reaction rates are nearly impossible to observe and identify, as their activation energies, i.e., the local maxima on the potential energy landscape, cannot be directly measured. However, it is not only the activation energy that is crucial to the progress of bond-forming and bond-breaking reaction steps. Charge redistribution and electron transfer during a chemical reaction also influence the possible pathways and outcomes, as well as the reaction rates. Among several processes, electron transfer in single molecules can

be initiated by spin-orbit coupling (SOC), which is a relativistic quantum effect due to the coupling of the electronic orbital angular momentum and spin. SOC happens between electronic states having potential surfaces that cross, approach each other, or run parallel in any nuclear degree of freedom.¹ The relevant geometries for these conditions may be far from equilibrium and represent a small subset of the accessible potential energy surfaces. Therefore, in many molecules consisting of light atoms, the role of SOC is considered to be rather minimal.²

It is at the heart of modern ultrafast science to trace and time the coupled non-adiabatic motion of electrons and nuclei in molecular dissociation processes that create transitional species, which make effective SOC possible and consequently impact the

mechanisms and outcomes of chemical reactions. In this study, we follow the creation of a short-lived molecular ion intermediate in either of two different electronic states. Moreover, we measure the transition probabilities of OD^+ leading to $\text{O}^+ + \text{D}$ or $\text{D}^+ + \text{O}$ dissociation, which are multi-step transitions governed by SOC and charge transfer.

The double ionization of (deuterated) water followed by the breakup of the dication is an ideal system in which to study such dynamics. It can lead to many fragmentation channels depending on the populated electronic state as well as on the rotational and vibrational modes of the molecule. The water dication can fragment into two bodies, $\text{D}^+ + \text{OD}^{+3-14}$ and $\text{D}_2^+ + \text{O}^+$,^{5,6,15-19} or dissociate into the competing three-body channels $\text{D}^+ + \text{D}^+ + \text{O}$ ^{7,12,14,20,21} and $\text{D}^+ + \text{O}^+ + \text{D}$.^{3-12,22-24} The latter, $\text{D}^+ + \text{O}^+ + \text{D}$, fragmentation channel is especially interesting as it is very rare compared to the $\text{D}^+ + \text{D}^+ + \text{O}$ breakup, even though the dissociation limits of these two channels are nearly degenerate. Production of the D^+ and O^+ fragments may happen directly following double ionization or proceed in a sequential way, i.e., by breaking one bond at a time, depending on the photon energy and the reaction pathway on the multi-dimensional potential energy surfaces (PESs). PESs and non-adiabatic coupling matrix elements, even for simple triatomic molecules, are not widely available for highly excited and dication states, as they are expensive to calculate, and, hence, the interpretation of the experimental results is challenging. We hasten to add that, for small molecules, alternative theoretical approaches are feasible.²⁵

In contrast to the rare $\text{D}^+ + \text{O}^+ + \text{D}$ channel, the direct and sequential (also known as concerted and stepwise, respectively) photodissociation of D_2O^{2+} into $\text{D}^+ + \text{D}^+ + \text{O}$ has been studied in great differential detail in a collaboration of experiment and theory.^{14,20,21} There have also been a number of earlier investigations in which the $\text{D}^+ + \text{O}^+ + \text{D}$ fragmentation channels have been observed. These studies included ion impact,^{7,8,22} electron impact,^{9-12,23} and single-photon double ionization.^{3-6,24} Yet none of these studies followed the dynamics of the transient reaction products. Instead, these experiments focused on identifying the fragmentation channels with, in some cases, speculations about the electronic states involved. They found contributions from either direct dissociation, indirect double ionization, or fragmentation via multi-step processes. Most of these studies obtained wide distributions of kinetic energy release (KER) upon fragmentation, covering energies from 5 eV up to 50 eV, which can be explained by the population of a variety of excited states of the dissociating D_2O^{2+} dication that eventually results in the final products mentioned above. Photoabsorption experiments close to the double ionization threshold^{3,4} yielded KER distributions centered at about 5 eV, which are considerably smaller than the KER values obtained in the x-ray regime^{5,6} or in electron-^{11,12} and ion-impact studies⁸ where Auger decay is the dominant process. The smaller KER studies must involve autoionization or a sequential dissociation process since the potential energy curves (PECs, i.e., cuts through the PESs, depicted in Fig. 2 of Ref. 20) of the states leading directly to $\text{D}^+ + \text{O}^+ + \text{D}$ fragmentation after double ionization of D_2O lie some 20 eV above the vertical double ionization threshold and are steeply repulsive. To maintain the present focus on pathways involving SOC in the molecular transient, we will not discuss autoionization further in this work and refer the reader to a separate publication by the authors for that study.²⁶

Despite all these investigations on the three-body fragmentation of D_2O into $\text{D}^+ + \text{O}^+ + \text{D}$, a complete picture of the sequential fragmentation processes at play in water after photo-double ionization (PDI) is still lacking. The evolution of intermediate species remains elusive because their transition rates cannot be easily identified and followed in the lab. In this report, the formation and dissociation of the transient OD^+ in its excited electronic states are observed, and the branching ratios (BR) for the production of two competing three-body channels, $\text{D}^+ + \text{D}^+ + \text{O}$ and $\text{D}^+ + \text{O}^+ + \text{D}$, are measured simultaneously and quantified by theory. Importantly, as we will see below, this branching ratio is the direct measure of the $\text{A } ^3\Pi \rightarrow \text{X } ^3\Sigma^- \rightarrow \text{B } ^3\Sigma^-$ transition probability in the dissociating OD^+ intermediate.

II. EXPERIMENT

The experiments were performed at the undulator beamline 10.0.1.3 at the Advanced Light Source (ALS) synchrotron ring at Lawrence Berkeley National Laboratory (LBNL) using 61.0 eV linearly polarized photons to investigate the fragmentation dynamics of D_2O molecular targets. The photon energy resolution was set to ~ 200 meV using the 10.0.1 monochromator.²⁷ Since the fragmentation channel of interest is very rare, the photon energy of 61.0 eV was chosen to be near the maximum of the PDI cross section of the water molecule. The experimental setup was similar to the one described in Ref. 14. In brief, a preheated supersonic gas jet consisting of D_2O vapor with a stagnation pressure of 2 bar was formed by heating the nozzle, the gas line, and the D_2O reservoir to temperatures of 125, 115, and 105 °C, respectively. The supersonic gas jet was collimated laterally by two skimmers (with 0.3 and 0.5 mm orifice diameters) and then crossed with a photon beam inside the particle 3D-momentum imaging spectrometer of a reaction microscope, a.k.a. the COLd Target Recoil Ion Momentum Spectroscopy (COLTRIMS) apparatus.²⁸⁻³⁰ A static electric field of 12.2 V/cm and a parallel magnetic field of 10.2 G guided electrons and ions to two micro-channel plate detectors, each equipped with a delay line readout,^{31,32} which were located at the opposite ends of the spectrometer. Electrons of up to 30 eV and ionic fragments of up to 22 eV were collected with 4π solid angle. The neutral O and neutral D fragments of the competing $\text{D}^+ + \text{D}^+ + \text{O}$ and $\text{D}^+ + \text{O}^+ + \text{D}$ reaction channels were not measured directly, but their momenta were derived using momentum conservation. Choosing D_2O as the target molecule enabled us to distinguish between PDI events from any residual H_2O background present in the vacuum chamber ($\approx 1.2 \times 10^{-8}$ Torr) and the supersonic gas jet. Moreover, the electric extraction field and spectrometer geometry were optimized to ensure that there was no overlap between the $\text{D}^+ + \text{O}^+ + \text{D}$ channel and the neighboring $\text{OH}^+ + \text{D}$ and $\text{OD}^+ + \text{D}^+$ two-body breakups in the PhotoIonPhotoIon COincidence (PIPICO) time-of-flight (TOF) spectrum (not shown here). Hence, the breakup channel of interest could be cleanly isolated in the PIPICO-TOF for further analysis.

Photoionization above the double ionization threshold leads to the dissociation of D_2O^{2+} , primarily to $\text{D}^+ + \text{D}^+ + \text{O}$ or $\text{D}^+ + \text{OD}^+$ (see Ref. 14 for the iso-energetic H_2O molecule). The $\text{D}^+ + \text{O}^+ + \text{D}$ three-body breakup channel is very weak. Nevertheless, in the present study, it could be identified and isolated with significant statistics for detailed analysis. The PDI yield branching

ratios of these three fragmentation channels are 47.5% for $\text{OD}^+ + \text{D}^+$, 51.8% for $\text{D}^+ + \text{D}^+ + \text{O}$, and 0.7% for $\text{D}^+ + \text{O}^+ + \text{D}$ with a *relative* error of $\leq 1\%$ each. The 47.5% for $\text{D}^+ + \text{OD}^+$ refers to the fraction that goes into long-lived rovibrational states of OD^+ (having lifetimes longer than the $4 \mu\text{s}$ TOF to the detector) and does not contribute to what is observed as three-body dissociation, while the 51.8% refers to the total fraction that fragments into $\text{D}^+ + \text{D}^+ + \text{O}$ either via direct or sequential breakup.

In general, the branching ratios are affected by the detection efficiencies of the D^+ , O^+ , and OD^+ ions on the MCP detector, which scale with E/\sqrt{m} of the particles. Yet, with an overall kinetic energy of around 2.2 keV gained in the particle extraction and post-acceleration regions of the imaging spectrometer, the ion detection efficiencies of all species measured are actually very similar (specifically, they are estimated to be ≈ 0.5 for O^+ and average to the same value for particles like H_2^+ and D^+ according to Ref. 33. Values for OD^+ are not known but are expected to be the same as for O^+).

III. SEQUENTIAL BREAKUP OF D_2O^{2+} INTO $\text{D}^+ + \text{O}^+ + \text{D}$

As mentioned in the introduction, the rare $\text{D}^+ + \text{O}^+ + \text{D}$ three-body breakup channel is further characterized by the competition between direct double ionization and autoionization processes.

The investigation of the autoionization process can be found in Ref. 26. In the present work, we isolate and analyze the direct PDI process. We achieve this by selecting the PDI events in which either of the two detected electrons exhibits a kinetic energy of $E_e \geq 2.5 \text{ eV}$, which primarily excludes low energy electrons that typically stem from double ionization involving auto-ionization (see Fig. 9 in Appendix A). In the next steps, we determine the relevant water dication states and fragmentation mechanisms at play, identify the sequential fragmentation events of interest (see Sec. III A), and then trace the dissociation pathways governed by SOC and charge transfer that lead to the final products $\text{D}^+ + \text{O}^+ + \text{D}$ (see Sec. III B). This enables us to retrieve the branching ratios for the electronically excited OD^+ transients that dissociate to $\text{O}^+ + \text{D}$ (see Sec. III C).

A. Electronic states and fragmentation mechanisms

Water Dication States: Absorbing a 61 eV photon in water can photo(double)ionize the target and populate several valence dication states (see the top panel in Fig. 1). The measured electron sum energy (see Fig. 10 in Appendix A) peaks around 17.2 eV and spans the six lowest excited dication states, 1^1A_1 , 1^1B_1 , 1^3A_2 , 1^3B_2 , 2^1A_1 , and 1^1A_2 . None of these correlate with the $\text{D}^+ + \text{O}^+ + \text{D}$ dissociation limit directly. In the investigation reported here, we mainly

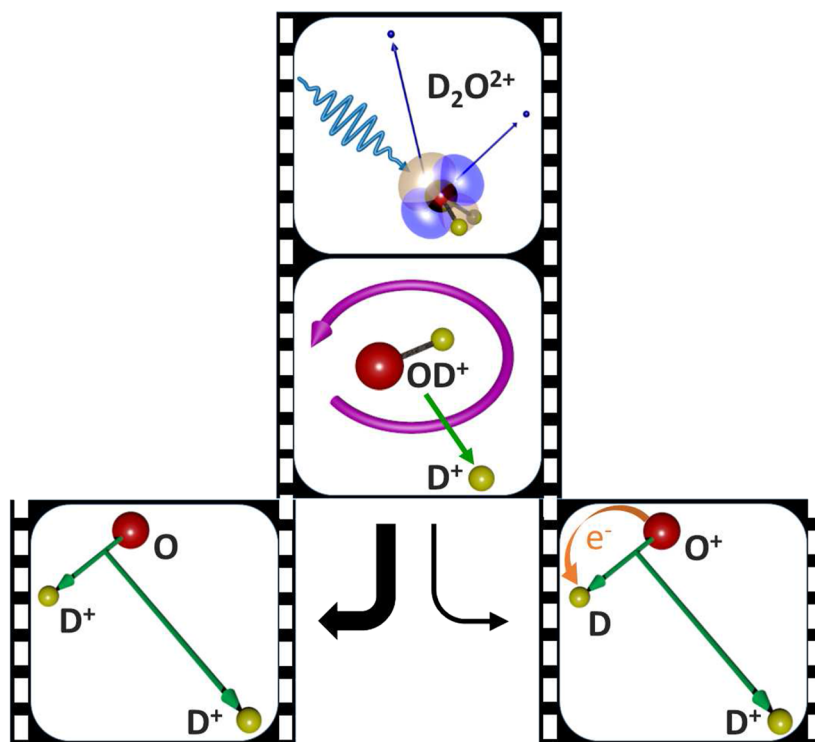


FIG. 1. Sketch of the PDI of D_2O populating several dication states (upper panel), followed by the two-body breakup into $\text{OD}^+ + \text{D}^+$, providing ample time for the transient OD^+ ion to rotate (middle panel) before either dissociating into $\text{D}^+ + \text{D}^+ + \text{O}$ or, less likely, electron transfer in the OD^+ intermediate takes place, which is producing $\text{D}^+ + \text{O}^+ + \text{D}$ (lower panel). Mainly the two water dication states 1^1B_1 and 2^1A_1 are populated, which feed the transient OD^+ ($a^1\Delta$, $b^1\Sigma^+$), respectively, in each fragmentation channel. These sequential dissociation routes can be exquisitely followed with the native fame analysis (see text).

focus on the 1^1B_1 and 2^1A_1 states, as they are known for having substantial contributions from sequential fragmentation²¹ and, therefore, are promising candidates to study the formation and dissociation of OD^+ intermediates. While the 1^1A_1 dication state might be considered as well because it undergoes predominantly (98.4%)²⁰ two-body breakup, it feeds the bound electronic ground state of OD^+ with insufficient internal energy to dissociate and yield notable three-body production.¹³ While focusing on the 1^1B_1 and 2^1A_1 dications, at this point, we cannot dismiss the possibility that there are other competing states and dissociation mechanisms that contribute to the $D^+ + O^+(^4S) + D$ production with similar excess energy and KER.

To determine the dissociation limit of the $D^+ + O^+ + D$ three-body breakup channel of interest, we plot in Fig. 2 the measured yield distribution of the total kinetic energy of the final products, i.e., the measured sum energy of the two electrons and the KER. The presented spectrum reveals that the direct PDI (black line) leading to $D^+ + O^+ + D$ ends up at a dissociation limit very close to the $D^+ + D^+ + O(^3P)$ breakup (purple line). We thus conclude that the measured total kinetic energy is correlated with the $D^+ + O^+(^4S) + D$ limit, which is nearly degenerate with the $D^+ + D^+ + O(^3P)$ limit (with an energy gap of ≈ 20 meV)^{34,35} and is well below the next nearest dissociation limit of $D^+ + O^+(^2D) + D$, which is expected to be 3.3 eV higher.

Fragmentation Routes: The sequential fragmentation of $D_2O^{2+}(1^1B_1, 2^1A_1)$ into $D^+ + D^+ + O(^3P)$ via $D^+ + OD^+$ has been recently investigated with a focus on two breakup paths.²¹ The second step in this sequential fragmentation process, namely the OD^+ dissociation to $D^+ + O(^3P)$, is driven by the SOC between the $a^1\Delta$ or $b^1\Sigma^+$ intermediate states and the $A^3\Pi$ state of OD^+ , the latter correlating with $O(^3P) + D^+$. We now seek to understand if additional SOC and charge transfer can alter the dissociation pathway leading to $D^+ + D^+ + O$ such that it can produce $D^+ + O^+ + D$. If sequential fragmentation into $D^+ + O^+ + D$ proceeds via the same transient OD^+ states, then a distinguishing mechanism must exist in the second breakup step, i.e., the OD^+ dissociation yielding $O^+(^4S) + D$

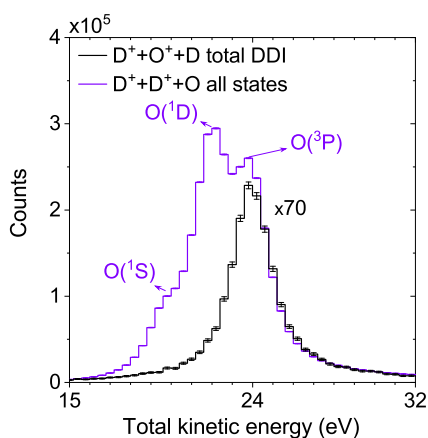


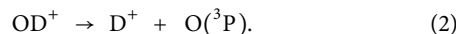
FIG. 2. Total kinetic energy $E_{sum} + KER$ for the $D^+ + D^+ + O$ breakup (purple line) and for the direct double ionization (DDI) process leading to $D^+ + O^+ + D$ (black line) upon PDI of D_2O with 61 eV photons. All error bars reflect one standard deviation of the statistical uncertainty.

instead of $D^+ + O(^3P)$. Next, we will track the OD^+ intermediate and quantify the ratio of each reaction channel produced during the dissociation process of this transient ion. This ratio is a direct measure of the transition probability leading to an OD^+ dissociation into $O^+ + D$ rather than $D^+ + O$.

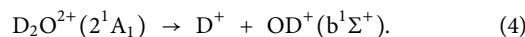
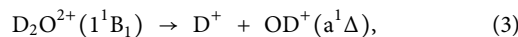
Sequential Dissociation: We now turn our attention to the investigation of the kinematics and energetics of this breakup process. Specifically, we are interested in the dynamics of the populated metastable states of the OD^+ intermediate, which were identified by Gervais *et al.*¹³ and examined in our recent joint experimental/theoretical study.²¹ Specifically, this sequential breakup in heavy water, observed in our experiment, begins with the two-body dissociation (see middle panel in Fig. 1),



followed by the dissociation of the metastable OD^+ transient ion (see bottom panel in Fig. 1),

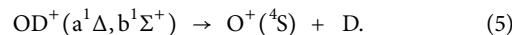


Between these two fragmentation steps, the intermediate excited OD^+ fragment rotates for a sufficient duration, i.e., longer than its rotational period (estimated to be about 1 ps using the rigid-rotor approximation for OD^+ at $R_{O-D} = 2$ a.u. and $j = 1$), in the fragmentation plane to erase any angular correlation between the two breakup steps, therefore leading to a uniform angular distribution of the $O-D^+$ dissociation direction [Eq. (2)] with respect to the OD^+-D^+ breakup axis of the first dissociation step [Eq. (1)]. We used this assumed full rotation of the OD^+ intermediate to extract the dynamics of this sequential fragmentation process and identified two specific pathways,²¹ namely



To reach the intermediate $D^+ + OD^+(a^1\Delta, b^1\Sigma^+)$ dissociation limit in this sequential breakup, the $D_2O^{2+}(1^1B_1, 2^1A_1)$ dication needs to undergo an asymmetric stretch starting from its symmetric C_{2v} geometry [for PECs, see Fig. 1(a) in Ref. 21]. We will be labeling the various water dication states by their symmetric (C_{2v}) spectroscopic designations, A_1 , A_2 , B_1 , and B_2 , with the understanding that at asymmetric geometries these should be replaced by their C_s designations, A' , A'' , A'' , and A' , respectively.

Both intermediate OD^+ states listed in Eqs. (3) and (4) can lead to the $D^+ + D^+ + O(^3P)$ final products via a spin-orbit mediated transition from the $a^1\Delta$ or $b^1\Sigma^+$ to the $A^3\Pi$ state of the metastable OD^+ fragment.^{13,36} However, it is also conceivable for a more exotic sequential process to occur, wherein the dissociating intermediate OD^+ molecule undergoes a different spin-orbit mediated transition, enabling dissociation to the $O^+ + D$ limit, namely



The latter fragmentation step listed in Eq. (5) results in the very rare three-body breakup $D^+ + O^+(^4S) + D$, which is the reaction channel of interest in this study (see bottom panel in Fig. 1).

To summarize, in this reaction, the 1^1B_1 and 2^1A_1 water dication states, which predominately dissociate in a sequential fashion to $D^+ + OD^+$, feed the electronically excited $a^1\Delta$ and $b^1\Sigma^+$ states of the OD^+ cation [see Eqs. (3) and (4)]. The PECs of the OD^+ ion and the vibrational levels of the $a^1\Delta$ and $b^1\Sigma^+$ states of the intermediate OD^+ ionic fragment, both correlating with the $D^+ + O(^1D)$ dissociation limit, are shown in Fig. 3.

We used the native frames analysis method^{21,37,38} to confirm these OD^+ cation states as active transients in our experiment, producing $D^+ + O^+ + D$ (see Appendix B for details about the method). The native frame analysis provides us with the emission angles and kinetic energies of the two separate dissociation steps and is thus well-suited for the following in-depth investigation of the sequential fragmentation. In Fig. 4, we plot all the measured $D^+ + O^+ + D$ events (except the ones associated with autoionization) as a function of the kinetic energy released in the second step, KER_{OD} , and the angle $\theta_{OD,D}$ between the conjugate momenta of the first dissociation step ($OD^+ - D^+$) and the second dissociation step ($O^+ - D$).

The broad angular distribution at low KER_{OD} , within the red rectangle in Fig. 4, resembles to some degree the distribution expected for a slow sequential breakup via an OD^+ intermediate, which rotates long enough in the fragmentation plane to yield a nearly uniform angular distribution, as expected in our native frames analysis. However, looking more closely, the projected angular distribution of the relevant events within the red rectangle in Fig. 4, shown in Fig. 5, is far from the expected flat distribution, $N(\theta_{OD,D}) = \text{constant}$, i.e., a uniform emission pattern in the fragmentation plane [compare with the uniform distribution in Fig. 2(c) in Ref. 21 for the $D^+ + D^+ + O$ channel and also see Fig. 11 in Appendix C]. Note that $\theta_{OD,D}$ is the angle between the conjugate momenta $P_{OD,D}$ and P_{OD} vectors, which define the fragmentation

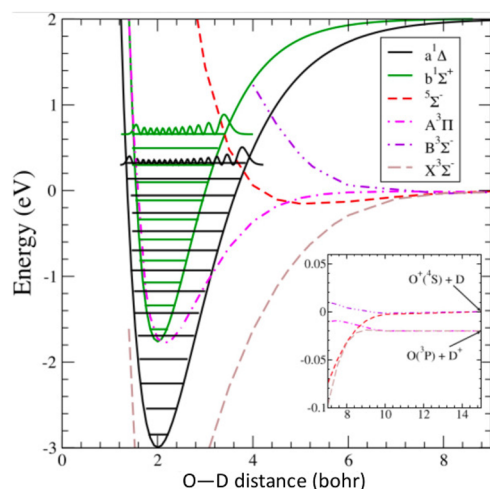


FIG. 3. Selected OD^+ PECs. The vibrational levels of the $a^1\Delta$, $b^1\Sigma^+$, and $1^1\Pi$ cation states are shown, as well as the PECs of the $5^3\Sigma^-$, $A^3\Pi$, $X^3\Sigma^-$, and $B^3\Sigma^-$ states. The dissociation limits of the latter four states are shown in the zoomed-in inset. The $a^1\Delta$, $b^1\Sigma^+$, and $1^1\Pi$ states all dissociate to $D^+ + O(^1D)$, 1.95 eV above the $O^+(^4S) + D$ dissociation limit. The zero of energy is taken to be the $O^+(^4S) + D$ dissociation limit.

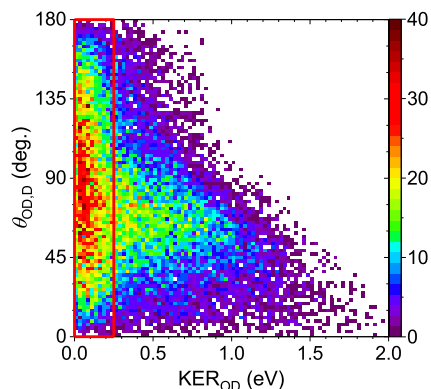


FIG. 4. All $D^+ + O^+ + D$ events of D_2O following direct PDI with 61 eV photons as a function of the kinetic energy release in the second breakup step, KER_{OD} , and the angle, $\theta_{OD,D}$, between the conjugate momenta of the first and second dissociation steps. The broad angular distribution at low KER_{OD} (i.e., within the red rectangle) is associated with the sequential breakup of D_2O^{2+} via the $D^+ + OD^+$ intermediate, followed by $OD^+ \rightarrow O^+ + D$ (i.e., resulting in the final products $D^+ + O^+ + D$). The events outside the red rectangle, which also yield $D^+ + O^+ + D$, stem from fragmentation Scenarios (1) and (3), described in this paper (see Appendix E), as well as from other dissociation mechanisms that will be discussed in detail elsewhere.

plane, and it represents the rotation of the second breakup direction relative to the first step within this plane (therefore, this angular distribution is plotted with equal bins in Figs. 4 and 5). This puzzling angular distribution is a consequence of the poor momentum resolution of the inferred neutral D fragment in our experiment and the very low KER_{OD} (≤ 0.25 eV) in the second step of this fragmentation process. In Fig. 5, we also show a simulated angular distribution that is expected once the experimental uncertainties

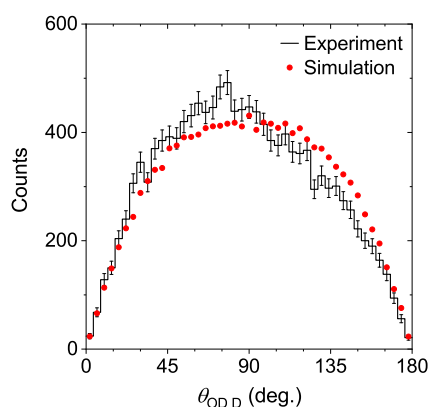


FIG. 5. Measured $D^+ + O^+ + D$ events with $KER_{OD} < 0.25$ eV upon PDI of D_2O with 61 eV photons as a function of the angle, $\theta_{OD,D}$, between the conjugate momenta of the first and second dissociation steps. The simulated data reflect the effect the experimental uncertainties have on this angular distribution for an assumed initial uniform distribution, i.e., $N(\theta_{OD,D}) = \text{constant}$ (see text and Appendix C). The degree of asymmetry of the distribution around its mean, i.e., the skewness, is 0.13 for the experimental distribution, while the simulated distribution is symmetric about 90° (i.e., skewness = 0). All error bars reflect one standard deviation of the statistical uncertainty.

affecting the expected uniform angular distribution are included (see [Appendixes C and D](#) for details). For the most part, this simulated distribution agrees with the measured one, therefore supporting the assignment of the events within the red rectangle in [Fig. 4](#) as sequential fragmentation via an OD^+ intermediate, which rotates in the fragmentation plane and has a KER_{OD} smaller than 0.25 eV. However, there is a noticeable mismatch between the experimental and simulated distributions of $\theta_{\text{OD,D}}$. The experimental distribution of $\theta_{\text{OD,D}}$ is asymmetric (skewness = 0.13), while the simulated distribution is centered at 90° . This small mismatch indicates the presence of another dissociation scenario at play leaking in from fragmentation mechanisms that are mainly present outside the red rectangle in [Fig. 4](#). As can be seen in [Fig. 4](#), events outside the red rectangle show $\theta_{\text{OD,D}}$ peaking between 45° and 90° , which is in agreement with the direction of the observed skewness in [Fig. 5](#).

Competing Minor Direct Fragmentation Scenario: Indeed, after careful examination, we also found that a direct three-body fragmentation into $\text{D}^+ + \text{O}^+ + \text{D}$, proceeding via symmetric OD stretch, is possible for direct PDI, populating the 1^1B_1 state [Scenario (1) in [Appendix E 1](#)]. It has similar energetics and kinematics in the lab frame and molecular frame as the sequential breakup and partly resides inside the red rectangle of [Fig. 4](#) (see [Appendix E 3](#) for details). The direct and sequential dissociation routes cannot be completely separated. This dissociation scenario, which is also present outside the red rectangle in [Fig. 4](#), is part of the reason for the observed skewness in [Fig. 5](#). Yet, the direct fragmentation involving SOC driven transitions from the 1^1B_1 state of D_2O^{2+} to either of the neighboring 2^3A_2 or 2^3B_2 triplet states, on which the water dication symmetrically stretches and finally reaches the $\text{D}^+ + \text{O}^+ + \text{D}$ dissociation limit, is a minor channel contributing 16% at most, compared to the sequential dissociation of this dication state; for completeness, the experimental and theoretical findings of this breakup scenario are described in [Appendix E 3](#).

Other fragmentation routes via intermediates such as $\text{OD}^{2+} + \text{D}$ or $\text{D}_2^+ + \text{O}^+$ as the first dissociation step are not energetically accessible, as observed from the measured electron sum energy. Hence, we can conclude that the sequential fragmentation process via the OD^+ transient is mainly governed by the dissociation pathways of the 1^1B_1 or 2^1A_1 states of the water dication to produce $\text{D}^+ + \text{O}^+ + \text{D}$.

While we have identified a slow sequential breakup as the most prominent dissociation pathway for the events in the red rectangle in [Fig. 4](#) ($\text{KER}_{\text{OD}} \leq 0.25$ eV), at this point we still cannot rule out the possibility that other states besides the two identified 1^1B_1 and 2^1A_1 dication states may contribute to these events.

B. Sequential dissociation pathways via $\text{D}^+ + \text{OD}^+$

Tracing the OD^+ Dissociation: In the following, we focus on the sequential fragmentation pathways of the D_2O^{2+} ($1^1\text{B}_1, 2^1\text{A}_1$) dication leading to a three-body breakup. After establishing that both reaction channels—the dominant $\text{D}^+ + \text{D}^+ + \text{O}$ and the rare $\text{D}^+ + \text{O}^+ + \text{D}$ —start out via the same sequential $\text{D}^+ + \text{OD}^+$ dissociation pathway, we now have to understand how additional SOC or charge transfer transitions in OD^+ ($a^1\Delta, b^1\Sigma^+$) produce $\text{O}^+(^4\text{S}) + \text{D}$ instead of $\text{D}^+ + \text{O}(^3\text{P})$. Returning to [Fig. 4](#), we note that sequential fragmentation via OD^+ yields a very low KER_{OD} in

the second step, i.e., the OD^+ dissociation into $\text{O}^+ + \text{D}$ (≤ 0.25 eV). This low KER_{OD} indicates that the process is most prominent near the dissociation threshold, and we only focus on these events in the following analysis.

Only two OD^+ states, namely $1^5\Sigma^-$ and $\text{B}^3\Sigma^-$, dissociate to ground-state $\text{O}^+(^4\text{S}) + \text{D}^{39,40}$ (see [Fig. 3](#)). Our initial hypothesis was a subsequent SOC transition from the $a^1\Delta$ or $b^1\Sigma^+$ states of OD^+ to the $1^5\Sigma^-$ state (see [Fig. 3](#)), which then produces $\text{O}^+(^4\text{S}) + \text{D}$, i.e., generates the final products $\text{D}^+ + \text{O}^+ + \text{D}$. However, this scenario is very unlikely due to the higher KER_{OD} associated with this dissociation (see [Fig. 3](#)) and the required inefficient SOC transition between the singlet and quintet states (see [Appendix E 2](#) for more details).

Spin-orbit mediated transitions from either the $a^1\Delta$ or the $b^1\Sigma^+$ states of OD^+ to the $\text{A}^3\Pi$ state, which we have shown to be a dominant route toward $\text{D}^+ + \text{O}(^3\text{P})$ dissociation,²¹ may lead to the $\text{O}^+(^4\text{S}) + \text{D}$ dissociation limit via additional transition(s). The $a^1\Delta$ or $b^1\Sigma^+$ to $\text{A}^3\Pi$ transitions are associated with a few tenths of picosecond lifetimes^{13,36} [corresponding to more than 100 vibrational periods of the relevant vibrational OD^+ ($a^1\Delta, b^1\Sigma^+$) states that are marked as black and green wavepackets in [Fig. 3](#), which are on the order of a few femtoseconds]. Recently, Hechtfischer *et al.*³⁴ studied the photodissociation of OH^+ just above the $\text{H}^+ + \text{O}(^3\text{P})$ dissociation limit with high spectroscopic resolution. They noticed dissociation occurring predominantly in the $\text{H}^+ + \text{O}$ but also in the $\text{O}^+ + \text{H}$ final products. The observation of the latter channel was attributed to a non-adiabatic coupling of the $\text{A}^3\Pi$ state of OH^+ , correlated with the $\text{H}^+ + \text{O}(^3\text{P})$ dissociation limit, to states that are dissociating to the nearly degenerate $\text{O}^+(^4\text{S}) + \text{H}$ limit. That led us to consider the direct coupling of OD^+ ($\text{A}^3\Pi$) to either $1^5\Sigma^-$ or $\text{B}^3\Sigma^-$. After careful examination, we concluded that this direct coupling cannot produce a significant amount of $\text{O}^+ + \text{D}$ relative to the $\text{D}^+ + \text{O}$ yield (see [Appendix E 2](#) for more details).

Another possibility is considering the ground $\text{X}^3\Sigma^-$ state as an additional OD^+ ($\text{X}^3\Sigma^-$) intermediate to facilitate the electron transfer. Both the $\text{A}^3\Pi$ and $\text{X}^3\Sigma^-$ states of OD^+ dissociate to $\text{D}^+ + \text{O}(^3\text{P})$; they are connected by a SOC, which, for intermediate to large R values, is, to a good approximation, just the fine-structure splitting of atomic oxygen and is R-independent. The $\text{X}^3\Sigma^-$ and $\text{B}^3\Sigma^-$ states, in turn, are more strongly coupled at large distances by electronic coupling than by the angular coupling that connects the $\text{A}^3\Pi$ and $\text{B}^3\Sigma^-$ states. O– D^+ charge-exchange between the X and $\text{B}^3\Sigma^-$ states has in fact been well-studied theoretically^{41–44} and experimentally,^{45,46} and the cross sections have been found to be significant near the threshold. Based on the calculations to be described below, we estimate the timescale of this $\text{A}^3\Pi \rightarrow \text{X}^3\Sigma^- \rightarrow \text{B}^3\Sigma^-$ dissociation sequence to be on the order of ≈ 700 ps.

In summary, we find that the most likely sequence of steps for sequential dissociation of D_2O^{2+} via the $\text{D}^+ + \text{OD}^+$ breakup, leading to $\text{O}^+(^4\text{S})$, involves the production of OD^+ ($a^1\Delta, b^1\Sigma^+$) intermediate ions from two-body dissociation on the 1^1B_1 and 2^1A_1 surfaces of the water dication, which then produce OD^+ ($\text{A}^3\Pi$) by SOC. An atomic spin-orbit interaction then strongly mixes the $\text{A}^3\Pi$ and $\text{X}^3\Sigma^-$ states, while an asymptotic electronic coupling between the $\text{X}^3\Sigma^-$ and $\text{B}^3\Sigma^-$ states triggers the charge-transfer that leads to the final reaction products $\text{D}^+ + \text{O}^+ + \text{D}$ [Scenario (2) in [Appendix E 1](#)]. The last step in this scenario is reminiscent of our earlier study of dissociative electron attachment to NH_3 molecules, where an asymptotic charge-transfer between $\text{NH}_2^- + \text{H}$ and $\text{H}^- + \text{NH}_2$ was

investigated.⁴⁷ Those states are split by 0.02 eV, just like the splitting in the present case of the OD⁺ dissociation, and we found in that case a transition probability of about 40%.

Competing Minor Dication State: Before proceeding with a quantitative examination of the efficiencies of the complex multi-step OD⁺(A³Π → X³Σ⁻ → B³Σ⁻) sequence of SOC and charge transfer transitions, we are now in a position to address the question raised above about the possibility of other dication states contributing to the O⁺ production at low-KER_{OD}. In particular, the 1³A₂ dication state, which lies energetically between the 1¹B₁ and 2¹A₁ states in the FC region, correlates directly with the intermediate OD⁺(A³Π) + D⁺ products. Since less than 1% of the 1³A₂ dication state decays via two-body breakup,¹³ it contributes predominantly via direct three-body fragmentation to the D⁺ + D⁺ + O production. Yet, the small percentage that does decay asymmetrically leads directly to OD⁺(A³Π) + D⁺, while the championed 1¹B₁ and 2¹A₁ states under study require a SOC to produce the A³Π state of OD⁺. Hence, further investigation with regard to this competing dissociation path is warranted. Figure 6 shows the electron sum energy that correlates with the production of D⁺ + O⁺ + D for low-KER_{OD} (≤0.25 eV). The distribution can be well fit using three states (employing only two states gave unsatisfactory fit results). The Gaussian width is extracted from the fit to the electron sum energy distribution for all events that result in the direct three-body channel D⁺ + D⁺ + O (not shown here). The difference between the widths of the 2¹A₁, 1³A₂, and 1¹B₁ dication states is very small (less than 10% disparity). Therefore, we used the same

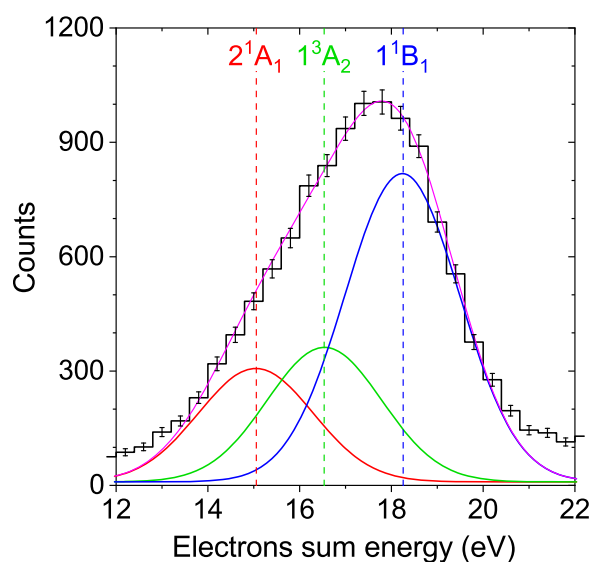


FIG. 6. Measured electron sum energy, E_{esum} , for the dication states leading to low-KER_{OD} (≤0.25 eV) contributions of the D⁺ + O⁺ + D fragmentation channel (black line) upon PDI of D₂O with 61 eV photons. The vertical lines indicate the positions of the dication states. Three Gaussians are fitted to the data. The first Gaussian fit (red line) represents the 2¹A₁ dication state (20.4 ± 1%), the second Gaussian fit (green line) represents the 1³A₂ dication state (24.2 ± 1.2%), the third Gaussian fit (blue line) represents the 1¹B₁ dication state (55.4% ± 0.9%), and the sum of all three Gaussians is shown as the magenta line. All error bars reflect one standard deviation of the statistical uncertainty.

widths for the fits of the three states. This procedure reveals that indeed the 1³A₂ dication state contributes around 24.2%. Since the SOC between the OD⁺(a¹Δ, b¹Σ⁺) and OD⁺(A³Π) cation states is the main cause for the sequential dissociation to be slow, removing that SOC will certainly make the breakup faster. Therefore, we can describe the breakup of D₂O²⁺(1³A₂) as a faster dissociation with little chance for at least one full revolution of the short-lived OD⁺(A³Π) transient, leading to OD⁺(A³Π)-D⁺ while populating continuum vibrational levels of OD⁺(A³Π) at or just above its dissociation limit in order to produce the low-KER_{OD}. The OD⁺(A³Π) transient cation state then connects to the OD⁺(X³Σ⁻) state by atomic SOC, followed by a charge-exchange to form OD⁺(B³Σ⁻), which then dissociates to O⁺ + D [Scenario (3) in Appendix E 1]. We will show elsewhere that the 1³A₂ dication state, which produces D⁺ + O⁺ + D exclusively by direct dissociation, affects events beyond the red rectangle in Fig. 4. It is the main contributor to the O⁺ production outside that rectangle, i.e., it produces D⁺ + O⁺ + D with a high-KER_{OD} (>0.25 eV). Nevertheless, the analysis of the slow sequential decay of the 1¹B₁ and 2¹A₁ dication states suffers from some contamination caused by the fast-sequential breakup of the 1³A₂ state, which we estimate to be 17% and 38%, respectively. These contributions are also causing the skewness observed in Fig. 5. They stem from the different angular distribution of the contributions outside the red rectangle in Fig. 4.

C. Dissociation branching ratios of transient electronically excited OD⁺

Theoretical Treatment: In the present context, we concluded that the X³Σ⁻ state of the OD⁺ intermediate facilitates the transfer from the A³Π to the B³Σ⁻ state of the transient ionic fragment. To test this hypothesis, we carried out a simplified time-dependent treatment of the OD⁺ dissociation dynamics initiated in the A³Π state. The formalism employed for this half-collision problem is analogous to the one used to study dissociative electron attachment.⁴⁸ The calculations were initiated by placing a vibrational wavefunction from either the a¹Δ or the b¹Σ⁺ state on the A³Π PEC of OD⁺. We chose vibrational levels with J = 0 at or above the A³Π dissociation limit (e.g., ν = 11 for a¹Δ and ν = 7 for b¹Σ⁺). We then solved the three-channel time-dependent Schrödinger equation, coupling the A³Π, X³Σ⁻, and B³Σ⁻ states, employing a constant SOC between the A and X states and electronic coupling between the X and B³Σ⁻ states, the latter taken from Ref. 41. From the half Fourier transform of the wavepackets on the three PECs evaluated at the dissociation limit, we obtained the final populations of the three electronic states and, hence, the O⁺ + D and D⁺ + O branching ratios as a function of KER_{OD}, bearing in mind that the X and A states both dissociate to the same [D⁺ + O(³P)] limit.

For initial vibrational wavepackets from either the a¹Δ or b¹Σ⁺ excited states of OD⁺, placed on the A³Π PEC, we find that the O⁺ + D and D⁺ + O branching ratios decrease as a function of KER_{OD} from threshold. For example, starting with the vibrational levels ν = 12 and 13 of the a¹Δ state, with corresponding KERs of 0.12 and 0.30 eV (ignoring the 0.02 eV energy difference between the D⁺ + O and O⁺ + D dissociation limits), the corresponding branching ratios are 0.023 and 0.018, respectively. We hasten to point out that this simplified treatment, in addition to ignoring the small asymptotic energy difference between the B and the A and X

dissociation limits in carrying out the time propagations, also ignores the effects of fine-structure splittings between the $O(^3P)$ states^{34,41,44} as well as rotational effects, all of which can be significant near threshold. For the vibrational level $\nu = 11$ of the $a^1\Delta$ state, which fortuitously lies very close to the $D^+ + O$ dissociation limit (see Fig. 3), we took the non-degeneracy of the $D^+ + O$ and $O^+ + D$ dissociation limits into account when choosing the energy differences between the initial vibrational level and the final asymptotic limits. As a result, the computed branching ratio for the $\nu = 11$ vibrational level of the $a^1\Delta$ state is 0.105. Unfortunately, in the case of the $b^1\Sigma^+$ state, there is no vibrational level close to the $D^+ + O$ dissociation limit, so the simplified model does not allow us to provide a threshold branching ratio for the $b^1\Sigma^+$ state. We shall see below that, despite the simplifications made, the dependence of the calculated branching ratios, BRs, on the KER_{OD} is in reasonable qualitative agreement with the experiment.

Branching Ratios of OD^+ Dissociations: On the experimental side, we turn again to the native frames analysis of the measured data, with which we are able to investigate the sequential breakup of D_2O^{2+} in great detail. We note that the dissociation via the two states of the OD^+ intermediate, $a^1\Delta$ and $b^1\Sigma^+$, can be separated in the experiment by the slanted line in the KER correlation map shown in Fig. 7(a) for the $D^+ + D^+ + O$ channel,²¹ which only represents the events from the sequential breakup. This KER correlation map shows this reaction channel's PDI yield as a function of the KER of the first step, $KER_{OD,D}$, and the KER of the second step, KER_{OD} . The ratios of the yields of these two fragmentation pathways, originating from the $D_2O^{2+}(1^1B_1, 2^1A_1)$ dications and leading to the $a^1\Delta$ and $b^1\Sigma^+$ states of the OD^+ intermediate, are around 37% and 63%, respectively, as extracted from the counts left and right of the slanted line in Fig. 7(a). In Fig. 7(b), we show a similar KER correlation map for the breakup generating the $D^+ + O^+ + D$ final products. The events with $KER_{OD} \leq 0.25$ eV (below the horizontal red dashed line) mainly represent the sequential dissociation processes in this reaction channel (compare to Fig. 4). With this identification, we can now compare the sequential breakup scenarios that are active in the $D^+ + D^+ + O$ channel [Fig. 7(a)] with the scenarios in the $D^+ + O^+ + D$ channel [Fig. 7(b)]. One can clearly see that in the latter case, the

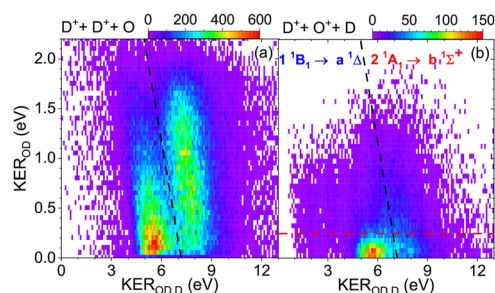


FIG. 7. KER correlation maps for the sequential fragmentation of $D_2O^{2+}(1^1B_1, 2^1A_1)$ after PDI of D_2O at 61 eV via $D^+ + OD^+$ followed by the dissociation of the intermediate molecular ion (a) $OD^+ \rightarrow D^+ + O$ (i.e., $D^+ + D^+ + O$ final products) (adapted from Ref. 21), and (b) $OD^+ \rightarrow O^+ + D$ (i.e., $D^+ + O^+ + D$ final products). The dashed lines separate the two states $a^1\Delta$ and $b^1\Sigma^+$ of the transient OD^+ at $KER_{OD,D} + KER_{OD} = 7.18$ eV.

transition via the $OD^+(a^1\Delta)$ state dominates the O^+ production at low KER_{OD} .

The fact that both final products of the OD^+ predissociation, namely $D^+ + O$ and $O^+ + D$, are measured simultaneously in their respective reaction channels, $D^+ + D^+ + O$ and $D^+ + O^+ + D$, allows us to compare their transition probabilities and, with this, the probability for an additional transition leading to $O^+ + D$ instead of $D^+ + O$. This comparison is made as a function of the energy above the dissociation limits within the common $KER_{OD} \leq 0.25$ eV window [note: we neglect the small energy difference between the $D^+ + O(^3P)$ and $O^+(^4S) + D$ dissociation limits shown in Fig. 3]. This is accomplished by computing the BRs for the $D^+ + O^+ + D$ channels, given by

$$BR(a^1\Delta, b^1\Sigma^+) = \frac{N(D^+ + O^+ + D)}{N(D^+ + O^+ + D) + N(D^+ + D^+ + O)}, \quad (6)$$

where the measured yields N are for the specific intermediate OD^+ states $a^1\Delta$ and $b^1\Sigma^+$. In order to remove the effect of the experimental resolution on the measured KER_{OD} distribution, we have used the simulated KER_{OD} (see Appendix C for details) for the calculation of the state-selective BRs in both reaction channels. We account for the possible systematic uncertainties in the measured branching ratios as follows: We note that we lose less than 0.5% of the $D^+ + D^+$ counts due to the multi-hit dead-time response of the detector for the $D^+ + D^+ + O$ channel, which for some events requires measuring two D^+ ions with similar time-of-flight that hit the detector at neighboring positions. Moreover, the counts of the $D^+ + O^+ + D$ reaction channel are corrected for the imperfect gate isolating the direct PDI from the autoionization mechanism, which has been achieved by monitoring the electron energy sharing (not shown here). Additionally, the pollution in the $D^+ + O^+ + D$ channel from the direct three-body fragmentation of the 1^1B_1 state, as discussed in Sec. III A, and from the fast-sequential breakup of the $D_2O^{2+}(1^3A_2)$ dication state, as discussed in Sec. III B, has been accounted for. After all these corrections, we estimate the remaining experimental relative uncertainty of the extracted BRs to be less than 10%, which has been added to the respective statistical errors.

In Fig. 8, we show the BRs, representing the probabilities to produce $D^+ + O^+ + D$ from the $a^1\Delta$ and $b^1\Sigma^+$ states of the excited OD^+ intermediate with respect to the sum of both sequential breakup channels, namely $D^+ + O^+ + D$ and $D^+ + D^+ + O$ [see Eq. (6)]. The BRs are a function of energy above the dissociation limit KER_{OD} , which is truncated for both the $D^+ + O^+ + D$ and $D^+ + D^+ + O$ channels at $KER_{OD} \leq 0.25$ eV. Since both the $a^1\Delta$ and $b^1\Sigma^+$ states of OD^+ dissociate via a SOC mediated transition to the $A^3\Pi$ state, which leads to the $D^+ + O(^3P)$ products, a sequence of additional transitions is needed to yield the observed $O^+(^4S) + D$ fragments. Assuming that the transition probabilities are products of the probabilities of each transition along the path, which means the transitions are independent from each other, the branching ratio is a measure of the $A^3\Pi \rightarrow X^3\Sigma^- \rightarrow B^3\Sigma^-$ transition sequence probability to produce the measured $O^+ + D$ reaction products (denoted hereafter as P_{A-X-B}). Quantitatively, $P_{A-X-B} = BR$ if $BR \ll 1$, otherwise, $P_{A-X-B} = BR/(1-BR)$. Moreover, as this BR is independent of the transition leading to the $OD^+(A^3\Pi)$ state, one can expect the BRs of the $a^1\Delta$ and $b^1\Sigma^+$ states of OD^+ as a function of KER_{OD} above the dissociation limit to be the same. Within the error bars, the observed

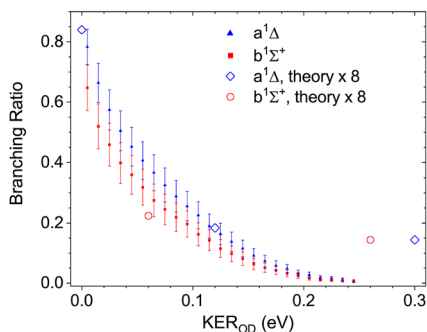


FIG. 8. The $D^+ + O^+ + D$ branching ratios with respect to the combined $D^+ + O^+ + D$ and $D^+ + D^+ + O$ production upon sequential dissociation of $D_2O_2^+$ ($1^1B_1, 2^1A_1$) according to Eq. (6) for the $OD^+(a^1\Delta)$ state (blue solid triangles and open diamonds) and the $OD^+(b^1\Sigma^+)$ state (red solid squares and open circles), separated in Fig. 7, for the same KER_{OD} range (≤ 0.25 eV).

near-congruence of the two measured BRs presented in Fig. 8 (solid blue triangles and red squares) confirms the interpretation above.

While the trends of the calculated BRs as a function of KER_{OD} are in reasonable agreement with the experiment, the theoretical BRs are roughly 8 times smaller than the experimental results, which is not very surprising given the somewhat coarse model employed here, as described above. However, in the case of the $a^1\Delta$ state, the theory results qualitatively confirm the experimental findings reasonably well. Figure 8 shows that for $KER_{OD} \leq 0.04$ eV, the likelihood of producing the reaction products $D^+ + O^+ + D$ is higher than the likelihood of generating $D^+ + D^+ + O$. This very low KER of OD^+ corresponds to a very slow dissociation and provides more time for efficient SOC, which is needed in this complex multi-step sequential dissociation process.

Finally, we note that our calculations with $J = 0$ were conducted for very few vibrational states, i.e., the ones within the relevant energy window. In contrast, the experiment smoothly spans the whole energy range because of the wide angular momentum distribution of the OD^+ intermediate.²¹ The explicit angular momentum (J) dependence of these multi-step transitions calls for further theoretical work.

IV. CONCLUSION AND SUMMARY

We identified two specific pathways in the rare dissociation of $D_2O_2^+$ into $D^+ + O^+ + D$. Both are initiated by populating either the 1^1B_1 or the 2^1A_1 electronic dication states by direct PDI, dissociating initially into $D^+ + OD^+$ intermediates. Applying our highly differential measurements and analysis methods in combination with coupled-channel time-dependent dynamics calculations, we have investigated state-selectively the possible sequential fragmentation mechanisms of the $D_2O_2^+$ dication, proceeding through the formation of excited OD^+ transients to feed the rare $D^+ + O^+ + D$ three-body breakup channel following PDI of water with a single 61 eV photon (see Fig. 1).

The first step of the dissociation pathway eventually leading to $D^+ + O^+ + D$, namely the breakup into $D^+ + OD^+$, is similar to our previous observation of the more prominent $D^+ + D^+ + O$ reaction

channel.²¹ The second step, specifically the predissociation of the $a^1\Delta$ and $b^1\Sigma^+$ states of the OD^+ transient ion, requires SOC to produce $OD^+(A^3\Pi)$, which starts dissociating toward the $D^+ + O(^3P)$ limit. However, to then generate the very rare reaction $D^+ + O^+ + D$ channel under investigation here, the subsequent pathway, diverting a small fraction of the events on the potential energy landscape toward the $D^+ + O^+ + D$ breakup, is more involved. It turns out that an additional atomic SOC connects the $OD^+(A^3\Pi)$ state to the $OD^+(X^3\Sigma^-)$ state, and the latter transient ion undergoes an asymptotic charge-transfer through electronic coupling to the $OD^+(B^3\Sigma^-)$ state, which eventually dissociates into $O^+(^4S) + D$, as these states are nearly degenerate for O–D distances greater than 6 bohrs. Apparently, this complex multi-step $A^3\Pi \rightarrow X^3\Sigma^- \rightarrow B^3\Sigma^-$ sequence of SOC and charge transfer transitions dominates over competing single transition paths like $A^3\Pi \rightarrow B^3\Sigma^-$ at low- KER_{OD} . An analogous electron transfer at similar intermediate distances (≈ 18 bohrs), without the need for SOC and hence of greater efficiency, has been observed recently in the PDI of NH_3 .⁴⁹

Evidently, upon PDI of heavy water creating $D_2O_2^+$, SOC effectively changes the course of the $D^+ + D^+ + O$ dissociation process toward the $D^+ + O^+ + D$ fragmentation channel by triggering charge redistribution and electron transfer in the sequential photodissociation route via OD^+ transients as a function of the KER (see Fig. 1). The key to the direct measurement of the $A^3\Pi \rightarrow X^3\Sigma^- \rightarrow B^3\Sigma^-$ transition probability in the transient OD^+ ion in our experiments is the simultaneous measurement of both sequential fragmentation channels, i.e., $D^+ + O^+ + D$ and $D^+ + D^+ + O$, combined with the fact that both dissociation paths have a common first step, namely the SOC transition to the intermediate $OD^+(A^3\Pi)$ fragment ion. The BR of the transient OD^+ ion to dissociate into $O^+(^4S) + D$ instead of $D^+ + O(^3P)$ varies with its KER and is similar for both $a^1\Delta$ and $b^1\Sigma^+$ states of the OD^+ intermediate. Apparently, feeding the $D^+ + O^+ + D$ reaction channel quickly becomes inefficient with increasing KER_{OD} of the dissociating OD^+ intermediate, as there is less time for effective SOC and the BRs drop to zero. On the other hand, under certain circumstances, the transient OD^+ ion dissociates more efficiently to $O^+ + D$ than $D^+ + O$. This can be seen in Fig. 8 for double ionization events where the kinetic energy release of the transient KER_{OD} is lower than 0.04 eV. For these very slow dissociation processes of $OD^+(a^1\Delta, b^1\Sigma^+)$, the branching ratios for producing $D^+ + O^+ + D$ exceed 0.5, i.e., they contribute more than the $D^+ + D^+ + O$ breakups.

ACKNOWLEDGMENTS

We acknowledge T. Weinacht for sparking our interest in this scarce water fragmentation channel. Work at LBNL was supported by the U.S. Department of Energy (DOE), Office of Science, Basic Energy Sciences (BES), under Award No. DE-AC02-05CH11231. This research used resources from the Advanced Light Source (ALS) and the National Energy Research Scientific Computing Center (NERSC), both DOE Office of Science User Facilities under Contract No. DE-AC02-05CH11231. In particular, we acknowledge NERSC Award Nos. BES-ERCAP-0020143 (theory) and BES-ERCAP-0019776 (experiment). We acknowledge the staff of the ALS, in particular beamline 10.0.1, for their outstanding support. The JRML personnel were supported by the U.S. Department of Energy

(DOE), Office of Science, Basic Energy Sciences (BES), under Award No. DE-FG02-86ER13491. UNR personnel acknowledge support from the National Science Foundation under Award Nos. NSF-1807017 and NSF-2208017. We are indebted to the RoentDek Company for long-term support with detector software and hardware.

AUTHOR DECLARATIONS

Conflict of Interest

The authors have no conflicts to disclose.

Author Contributions

W.I. and Th.W. designed the experiment. W.I., Th.W., K.A.L., B.G., J.B.W., B.J., D.C., V.D., T.S., and D.S.S. conducted the beam time and acquired the experimental data at the Advanced Light Source. W.I. and T.S. analyzed the data. T.N.R., A.E.O., and Z.L.S. performed the calculations. W.I., T.N.R., I.B.-I., and Th.W. wrote the manuscript with significant review and editing by T.S., D.S.S., C.W.M., and R.R.L., which all co-authors approved. W.I., T.S., I.B.-I., T.N.R., C.W.M., and Th.W. created the figures.

W. Iskandar: Conceptualization (equal); Formal analysis (lead); Investigation (equal); Visualization (lead); Writing – original draft (lead); Writing – review & editing (equal). **T. N. Rescigno:** Formal analysis (equal); Investigation (equal); Visualization (equal); Writing – original draft (equal); Writing – review & editing (equal). **A. E. Orel:** Formal analysis (equal); Investigation (equal); Writing – review & editing (equal). **T. Severt:** Formal analysis (equal); Investigation (equal); Visualization (equal); Writing – review & editing (equal). **K. A. Larsen:** Investigation (equal); Writing – review & editing (supporting). **Z. L. Streeter:** Investigation (supporting); Writing – review & editing (supporting). **B. Jochim:** Investigation (supporting). **B. Griffin:** Investigation (supporting). **D. Call:** Investigation (supporting). **V. Davis:** Investigation (supporting); Writing – review & editing (supporting). **C. W. McCurdy:** Funding acquisition (equal); Investigation (supporting); Writing – review & editing (equal). **R. R. Lucchese:** Funding acquisition (equal); Investigation (supporting); Writing – review & editing (supporting). **J. B. Williams:** Investigation (supporting). **I. Ben-Itzhak:** Funding acquisition (equal); Investigation (equal); Supervision (equal); Visualization (supporting); Writing – original draft (equal); Writing – review & editing (equal). **D. S. Slaughter:** Conceptualization (supporting); Funding acquisition (equal); Investigation (equal); Project administration (equal); Supervision (equal); Writing – review & editing (lead). **Th. Weber:** Conceptualization (lead); Data curation (lead); Funding acquisition (lead); Investigation (lead); Project administration (lead); Supervision (equal); Writing – original draft (equal); Writing – review & editing (equal).

DATA AVAILABILITY

The data that support the findings of this study are available from the corresponding author upon reasonable request.

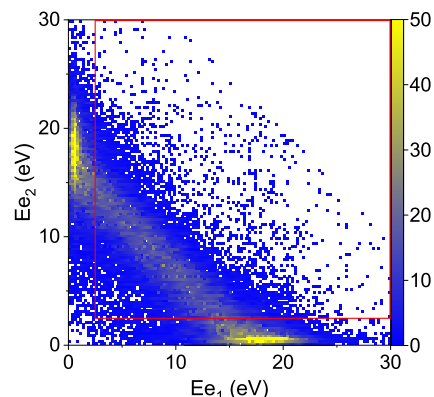


FIG. 9. Electron energy correlation map for all photo double ionization events leading to the $D^+ + O^+ + D$ fragmentation channel at 61 eV. The contributions from autoionization have been excluded by gating on the events in the red rectangle.

APPENDIX A: WATER DICATION STATES

The electron-electron energy correlation map for all photo double ionization events leading to the $D^+ + O^+ + D$ fragmentation channel at 61 eV is shown in Fig. 9. In the remainder of the analysis, the autoionization channel is excluded by taking only the events in the red rectangle into account.

By plotting the measured sum energy of both detected electrons, we can identify which water dication states have been populated in the direct double ionization (DDI). The vertical lines in Fig. 10 indicate the positions of the dication states at the equilibrium geometry of the neutral water molecule derived from the potential energy curves in Ref. 20. Note that the calculations of Streeter *et al.* in Ref. 20 incorrectly place the $H^+ + H^+ + O$ asymptote 0.2 eV above the $H^+ + O^+ + H$ limit. This error is related to the difficulty of calculating the ionization potential (IP) of atomic oxygen (13.618 eV) relative to that of hydrogen (13.598 eV) and

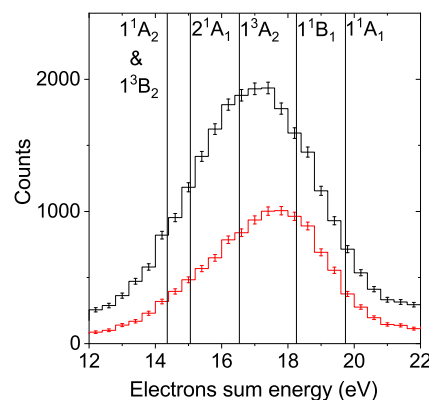


FIG. 10. Electron sum energy, $E_{e_{sum}}$, for the direct double ionization (DDI) process leading to the $D^+ + O^+ + D$ fragmentation channel. All error bars reflect one standard deviation of the statistical uncertainty. Black lines and symbols: all KER_{OD} contributions. Red lines and symbols: for $0 \leq KER_{OD} \leq 0.25$ eV.

TABLE I. Electronic states of water dications and their electronic configurations in C_{2v} symmetry, the two- and three-body dissociation products, and thermochemical thresholds for the generated products. The electronic configuration of neutral water is given as $1a_1^2 2a_1^2 1b_2^2 3a_1^2 1b_1^2$.

C_{2v} sym.	Electronic configuration	2-Body dissoci. limit	3-Body dissoci. limit	Thermochemical threshold (eV)
X^3B_1	$(3a_1 1b_1)^{-1}$	$OD^+(X^3\Sigma^-) + D^+$	$D^+ + D^+ + O(^3P)$	36.86
1^1A_1	$(1b_1)^{-2}$	$OD^+(a^1\Delta) + D^+$	$D^+ + D^+ + O(^1D)$	38.83
1^1B_1	$(3a_1 1b_1)^{-1}$	$OD^+(a^1\Delta) + D^+$	$D^+ + D^+ + O(^1D)$	38.83
1^3A_2	$(1b_2 1b_1)^{-1}$	$OD^+(A^3\Pi) + D^+$	$D^+ + D^+ + O(^3P)$	36.86
2^1A_1	$(3a_1)^{-2}$	$OD^+(b^1\Sigma^+) + D^+$	$D^+ + D^+ + O(^1D)$	38.83
1^1A_2	$(1b_2 1b_1)^{-1}$	$OD^+(^1\Pi) + D^+$	$D^+ + D^+ + O(^1D)$	38.83
1^3B_2	$(1b_2 3a_1)^{-1}$	$OD^+(A^3\Pi) + D^+$	$D^+ + D^+ + O(^3P)$	36.86
2^3A_2	$(1b_2 1b_1 3a_1)^{-1} 4a_1^1$	$OD^+(B^3\Sigma^-) + D^+$	$D^+ + D + O(^4S)$	36.88
2^3B_1	$(3a_1)^{-2} (1b_1)^{-1} 4a_1^1$	$OD^+(B^3\Sigma^-) + D^+$	$D^+ + D + O(^4S)$	36.88

has been taken into account here. The black line and symbols represent the electron sum energy distribution for DDI events (no restriction on KER_{OD}), while the red line and symbols show the events with $KER_{OD} \leq 2.5$ eV, which stem from mostly the sequential breakup of the OD^+ intermediate into $O^+ + D$ (see also Fig. 6 and related text for further analysis). The electronic configurations (in C_{2v} geometry), the two-body and three-body dissociation limits of the states, as well as the thermochemical thresholds are given in Table I.

APPENDIX B: NATIVE FRAMES ANALYSIS METHOD

The native frames analysis method is based on the use of the conjugate momenta of the Jacobi coordinates, which describe the relative positions of the three fragments.^{21,37,38} For D_2O fragmenting into $D^+ + O^+ + D$ via the intermediate $D^+ + OD^+$, the conjugated momentum associated with the first breakup step is given by

$$\mathbf{P}_{OD_{II},D_I} = \frac{m_{OD}}{M} \mathbf{P}_{D_I} - \frac{m_D}{M} [\mathbf{P}_{D_{II}} + \mathbf{P}_O], \quad (B1)$$

where \mathbf{P}_{D_I} and \mathbf{P}_O are the measured momenta of the D^+ and O^+ fragments, respectively, while $\mathbf{P}_{D_{II}}$ is the momentum of the neutral D fragment evaluated from momentum conservation. (Note that in the equations, we denote the D^+ and D fragments as D_I and D_{II} , respectively.) In this case, m_D is the mass of D^+ , m_{OD} is the mass of OD^+ , and M is the mass of the D_2O^{2+} dication.

Similarly, the conjugate momentum associated with the second breakup step is

$$\mathbf{P}_{OD_{II}} = \mu_{OD} \left[\frac{\mathbf{P}_{D_{II}}}{m_D} - \frac{\mathbf{P}_O}{m_O} \right], \quad (B2)$$

where μ_{OD} is the reduced mass of OD^+ . The angle between these two vectors, θ_{OD_{II},D_I} , is evaluated from the scalar product of the conjugate momenta given in Eqs. (B1) and (B2). Finally, the KERs of the first and second steps are given by $KER_{OD_{II},D_I} = \mathbf{P}_{OD_{II},D_I}^2 / 2\mu_{OD,D}$ (where $\mu_{OD,D}$ is the reduced mass of $D^+ - OD^+$) and $KER_{OD_{II}} = \mathbf{P}_{OD_{II}}^2 / 2\mu_{OD}$, respectively.

APPENDIX C: MONTE-CARLO SIMULATION

We perform a Monte-Carlo simulation to determine the impact of the experimental uncertainties on the measured distribution of the angle between the conjugate momenta given in Eqs. (B1) and (B2), $N(\theta_{OD,D})$, i.e., the direction of the assumed two breakup steps, as well as the KER in the second step. As this KER_{OD} approaches zero, it becomes harder to define the angle $\theta_{OD,D}$, and this effect is also addressed by this simulation. Specifically, we assume that the distribution is uniform, i.e., $N(\theta_{OD,D}) = \text{constant}$, and simulate how it becomes distorted due to the finite experimental resolution. To achieve this, we first compute the momenta of the three fragments upon dissociation using the measured KER associated with each step of the sequential breakup and span $\theta_{OD,D}$ randomly over the whole angular range.

The angular and energy resolution of the detected fragment ions are affected by (a) the size of the interaction volume defined by the overlap between the synchrotron light and gas jet beam ($\approx 1.0 \times 0.3 \times 0.3$ mm³), (b) the temperature of the supersonic gas target (≈ 50 K parallel and ≈ 15 K perpendicular to the jet propagation direction), and (c) the time (≈ 0.5 ns) and position (≈ 0.25 mm) uncertainties of our particle detectors.

We generate a random distribution of the initial positions of the D_2O molecules to match the interaction volume defined by the crossing of the molecular jet and synchrotron beam, given explicitly by the boundary condition (a). To satisfy condition (b), we generate a center-of-mass (CM) velocity distribution for the D_2O molecules in the supersonic jet of our COLTRIMS setup. Next, using this “initial” CM-velocity and the point of origin of each fragment, combined with the $N(\theta_{OD,D}) = \text{constant}$ distribution, we compute its impact time and position on the detector by solving the equations of motion in our COLTRIMS spectrometer. Then, we add the uncertainty due to the detector resolution, given in point (c) above, to the simulated impact data. Using the resulting dataset, we compute the momenta of the D^+ and O^+ fragments for each event (i.e., single molecule) by applying the same algorithm as for the measured data. Likewise, the momentum of the neutral D fragment is computed using momentum conservation. The resulting simulated momenta now include the main experimental uncertainties listed in the experimental broadening conditions (a)–(c) above.

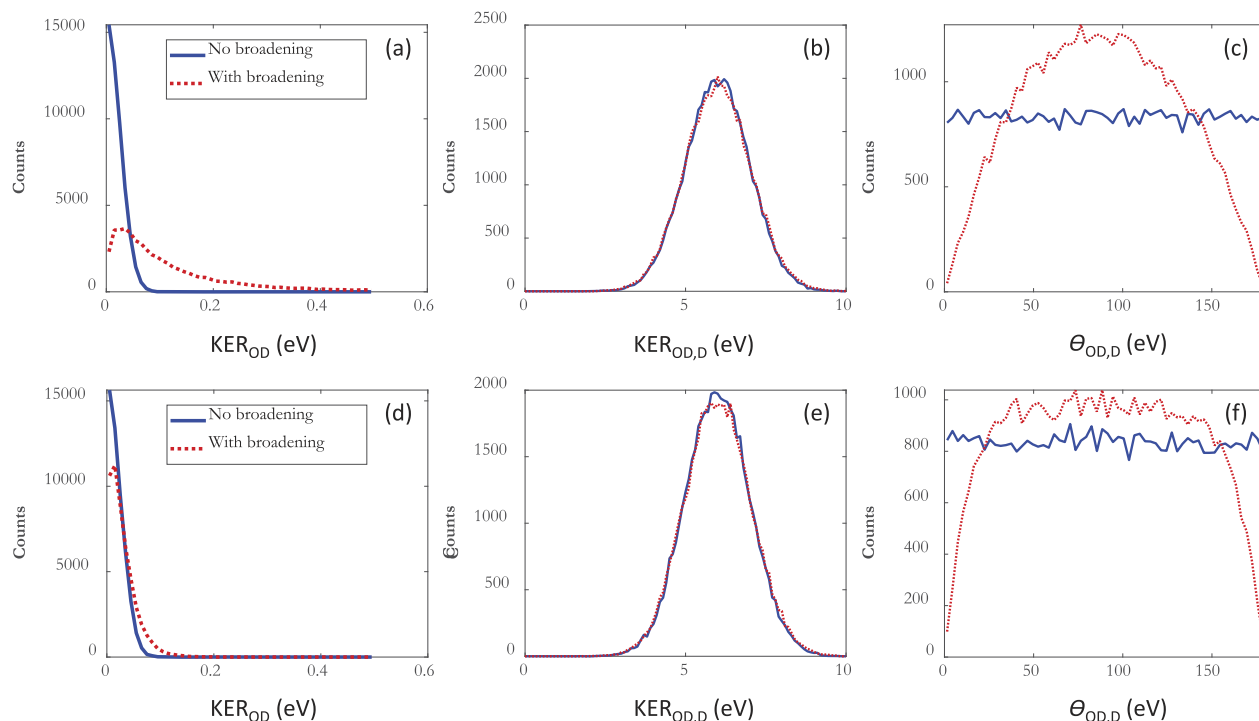


FIG. 11. Simulations of the relevant observables of the native frames analysis of the $D^+ + O^+ + D$ (a)–(c) and $D^+ + D^+ + O$ (d)–(f) fragmentation channels with (red dashed curve) and without (solid blue curve) experimental broadening (see text) show the uncertainties effect on the KER_{OD} (a), (d), $KER_{OD,D}$ (b), (e), and $\theta_{OD,D}$ (c), (f) distributions.

This process is repeated for about the same number of events as in the measured dataset to achieve similar statistical quality as in the experiment.

The simulation, which includes the experimental resolutions and yields a non-uniform distribution that is similar to the measured spread, indicates significant distortion of the expected $N(\theta_{OD,D}) = \text{const.}$ angular distribution, as shown in Fig. 5. The near congruence of the observed and simulated distributions suggests that the measured $\theta_{OD,D}$ spread represents what one should expect for a uniform angular distribution in $\theta_{OD,D}$ of a sequential fragmentation via an intermediate transient molecule, i.e., OD^+ rotating in the fragmentation plane, under the influence of the uncertainties of our experiment [for comparison, see the uniform distribution in Fig. 2(c) in Ref. 21 for the $D^+ + D^+ + O$ channel]. This notable distortion of the angular distribution is rooted in the momentum of the detected O^+ ion, which is on the order of the D^+ momentum but results in low kinetic energy of this heavy fragment and, hence, little excursions on the ion detector and a small spread in time-of-flight.

The KER_{OD} distribution of the second fragmentation step is also affected by the experimental resolutions, becoming broader than it should be. This broadening was corrected for the BR data shown in Fig. 8.

In contrast to the large distortions in the $D^+ + O^+ + D$ channel, the same simulation for the $D^+ + D^+ + O$ fragmentation channel, measured simultaneously, i.e., affected by the same

experimental uncertainties, demonstrates that distortions of the reported uniform angular distribution, $N(\theta_{OD,D})$, and the second breakup step KER_{OD} distribution [see Fig. 2(c) in Ref. 21] are significantly smaller. This difference between the $D^+ + D^+ + O$ and the $D^+ + O^+ + D$ channels is due to the much better momentum resolution of the detected D^+ ions as compared to the O^+ ions in our measurements.

To visualize this distortion, we show in Fig. 11 how the simulated uncertainties affect the relevant observables of the native frames analysis while assuming the same KER_{OD} and $KER_{OD,D}$ distributions for both fragmentation channels. We find that, while the KER_{OD} distribution broadens in panel (a), the assumed flat (uniform) $\theta_{OD,D}$ angular distribution for the $D^+ + O^+ + D$ channel in panel (c) becomes peaked at around 90° . We see no effect of the simulated uncertainties on the $KER_{OD,D}$ distribution in panel (b) for the $D^+ + O^+ + D$ fragmentation. In contrast to the $D^+ + O^+ + D$ fragmentation, the broadening of the KER_{OD} distribution in the $D^+ + D^+ + O$ reaction channel is barely noticeable in panel (d). The assumed flat (uniform) $\theta_{OD,D}$ angular distribution remains flat in most parts but develops dips for very small and large angles of the $D^+ + D^+ + O$ fragmentation in panel (f). In summary, the same experimental uncertainties result in significantly smaller distortions of the expected flat (uniform) angular distribution $\theta_{OD,D}$ between the conjugate momenta of the two fragmentation steps and the KER_{OD} of the second dissociation step in the latter reaction channel.

APPENDIX D: EXPERIMENTAL SHIFTS AND BROADENING—IMPACT OF THE EXPERIMENTAL RESOLUTION ON THE RELATIVE ANGLES OF THE FRAGMENTS

For the discussion of the kinematics of the considered dissociation routes, the angular resolutions of the fragments have to be taken into account. In the lab frame, the average momentum uncertainty of O^+ ions is approximately ± 1.9 a.u., while the uncertainty for the D^+ ion is about ± 0.7 a.u. The derived momentum of the neutral D fragment is low and peaks around 5.8 a.u. It has a significant momentum uncertainty of about ± 2.3 a.u., which has a large impact on the corresponding angular distribution. While integrating over the direction of the polarization vector, we define the molecular breakup frame via the measured momenta of the three heavy fragments in the laboratory frame, which establish a plane (similar to a Newton plot). The azimuthal relative angles $\phi_{A,B}$ between the fragments A and B are measured around the normal of this plane [$\arctan(p_A/p_B)$] and shown in Fig. 12. The uncertainties of the relative angles between D^+ and D and between O^+ and D are on average $\pm 31^\circ$ and $\pm 33^\circ$, respectively, while the uncertainty of the relative angle between O^+ and D^+ ions is notably better (about $\pm 3^\circ$).

A deconvolution, comprising the finite momentum resolution of the measured fragment pair angles ϕ_{O^+,D^+} , which peak at 175° in Fig. 12, yields sharp distributions shifted to 180° (not shown here). The deconvoluted $\phi_{D^+,D}$ and $\phi_{O^+,D}$ angular distributions peak at 180° and 0° , respectively, but are notably broader. These observed large shifts in the measured relative angles $\phi_{D^+,D}$ and $\phi_{O^+,D}$ in Fig. 12 are to be expected for particles that fly in the opposite or the same direction when the uncertainty of the center-of-mass-momentum of this subsystem is on the order of one of their momentum vectors. This is because the finite resolution in these emission scenarios provides ample phase space to redistribute yield away from a strict parallel or anti-parallel orientation of the momentum vectors, which are scarce combinations to begin with due to the small solid angle. The situation is different for relative angles larger than 0° and smaller than 180° because the solid angle, and, hence, the yield

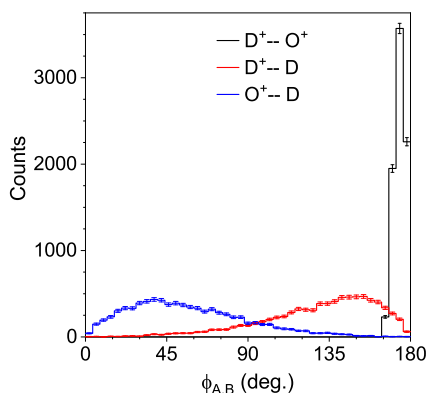


FIG. 12. Relative angles $\phi_{A,B}$ in the molecular breakup plane of D_2O^{2+} between fragment pairs D^+ and O^+ (black), D^+ and D (red), and O^+ and D (blue) for the $KER_{OD} \leq 0.25$ eV feature, marked as the red rectangle in Fig. 4. All error bars represent one standard deviation of statistical uncertainty.

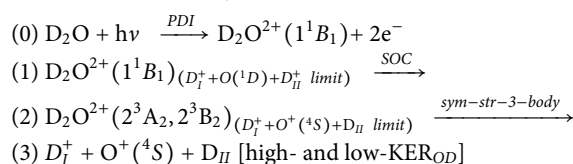
for these orientations of the momentum vectors, is much larger. Consequently, the finite lab frame angular resolutions mentioned above will mainly result in a broadening of the relative angles but little to no shift for the measured relative angles of fragment pairs approaching 90° that are contributing to the events inside the red rectangle and beyond in Fig. 4.

APPENDIX E: CONSIDERED DISSOCIATION MECHANISMS OF THE 1^1B_1 , 2^1A_1 , AND 1^3A_2 WATER DICATION STATES

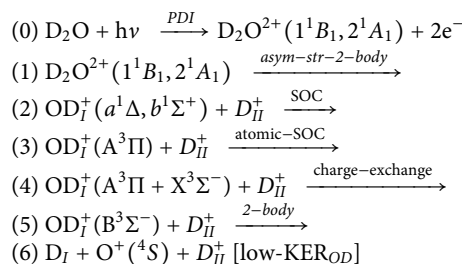
1. Overview of fragmentation scenarios

The D fragments, which are subject to electron transfer, are distinguished by as D_{II} , while D_I represents the D^+ ions that remain unaffected.

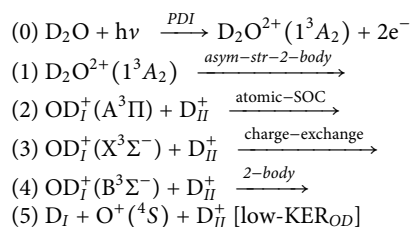
SCENARIO (1): Direct Fragmentation



SCENARIO (2): Slow Sequential Fragmentation



SCENARIO (3): Fast Sequential Fragmentation



2. Alternative less likely dissociation routes of the $OD^+(a^1\Delta, b^1\Sigma^+)$ intermediate in Scenario (2)

The dissociation of the $OD^+(a^1\Delta, b^1\Sigma^+)$ intermediate into $O^+ + D$ to yield $D^+ + O^+(^4S) + D$ in the measurement could take place in several ways. Bearing in mind that only two OD^+ states, namely $1^5\Sigma^-$ and $B^3\Sigma^-$, dissociate to ground-state $O^+(^4S) + D$ ^{39,40} (see Fig. 3), and assuming either $D_2O^{2+}(1^1B_1$ or $2^1A_1)$ dications to dissociate into $D^+ + OD^+(a^1\Delta$ or $b^1\Sigma^+)$ in the first step, our initial hypothesis was a subsequent SOC transition from the $a^1\Delta$ or $b^1\Sigma^+$ states of OD^+ to the $5^5\Sigma^-$ state (see Fig. 3), which then produces $O^+(^4S) + D$, i.e., generates the final products $D^+ + O^+ + D$. Considering the lowest PECs of the OD^+ intermediate ion, shown in Fig. 3, we then expect a direct predissociation from the $a^1\Delta$ and $b^1\Sigma^+$

states to the final $1^5\Sigma^-$ state, mediated by SOC, to be strongest near the crossings between these PECs. The KERs associated with these crossings are expected to peak around 0.31 and 0.67 eV, respectively (see Fig. 3), while the measured KER associated with this dissociation step is much lower, specifically peaking around 0.06 eV. This reason, along with the fact that SOC between singlet and quintet states is quite small, leads us to conclude that these pathways are clearly not the dominant ones.

As a direct transition of the $\text{OD}^+(\text{a}^1\Delta, \text{b}^1\Sigma^+)$ to the $1^5\Sigma^-$ state seems unlikely, we then took into account that a transition to the $\text{OD}^+(\text{A}^3\Pi)$ takes place first. Yet, spin-orbit mediated transitions from either the $\text{a}^1\Delta$ or the $\text{b}^1\Sigma^+$ states of OD^+ to the $\text{A}^3\Pi$ state, which we have shown to be a dominant route toward $\text{D}^+ + \text{O}(\text{P})$ dissociation,²¹ may lead to the $\text{O}^+(\text{S}) + \text{D}$ dissociation limit by several pathways. One possibility is an additional spin-orbit transition between the $\text{A}^3\Pi$ and the final $1^5\Sigma^-$ states along the dissociation path. This can be viewed as a third step along this sequence of fragmentation steps, which starts with D_2O^{2+} breaking up to $\text{D}^+ + \text{OD}^+$, followed by the predissociation of the OD^+ intermediate via the $\text{A}^3\Pi$ state toward the $\text{D}^+ + \text{O}(\text{P})$ limit, and ends with $\text{A}^3\Pi \rightarrow 1^5\Sigma^-$, i.e., a spin-orbit mediated transition that leads to the $\text{O}^+(\text{S}) + \text{D}$ dissociation limit of interest in this work. Hechtfisher *et al.*,³⁴ however, pointed out that the $\text{A}^3\Pi$ and $1^5\Sigma^-$ states only interact through second-order SOC, which they, therefore, did not consider in their detailed modeling of near-threshold photodissociation of OH^+ .

Instead of this second SOC mediated path, which is very unlikely to take place as the states involved in the transitions have different symmetry as well as spin, an electron transfer in the fragmenting OD^+ intermediate between the $\text{A}^3\Pi$ state, dissociating into $\text{D}^+ + \text{O}(\text{P})$, and the $\text{B}^3\Sigma^-$ state, dissociating into the measured $\text{O}^+(\text{S}) + \text{D}$, appears more probable. These states run parallel, separated by ≈ 0.02 eV, for O–D distances greater than 6 bohrs toward their respective limits, as seen in Fig. 3, and, hence, provide ample time for the charge transfer. A non-adiabatic transition between the Π and Σ states is facilitated by a matrix element describing the electronic orbital angular momentum coupling, as laid out by Wolniewicz *et al.*⁵⁰ The matrix element falls off as $1/R^2$. We modified our structure codes to include this property and found that at ≈ 6 bohrs, the coupling matrix element is ≈ 0.025 a.u. However, since this angular coupling derives from the nuclear kinetic energy, it enters the Hamiltonian with a factor of one over the reduced mass ($1/\mu_{\text{OD}} = 1/3264$ a.u.) and is hence very small. Wavepacket calculations confirmed that this angular coupling resulted in a negligible transfer of population to the $\text{O}^+(\text{S}) + \text{D}$ channel. As the likelihoods for the above contemplated dissociation routes appear to be very small, we were left with considering a complex multi-step $\text{OD}^+(\text{a}^1\Delta \text{ or } \text{b}^1\Sigma^+ \rightarrow \text{A}^3\Pi \rightarrow \text{X}^3\Sigma^- \rightarrow \text{B}^3\Sigma^-)$ sequence of SOC and charge transfer transitions as described in the main text (see Sec. III B).

3. Direct breakup of $\text{D}_2\text{O}^+(\text{1}^1\text{B}_1, \text{2}^1\text{A}_1)$ into $\text{D}^+ + \text{O}^+ + \text{D}$ for Scenario (1)

In the following, we describe why a second dissociation scenario for the 1^1B_1 dication state, i.e., the direct fragmentation into $\text{D}^+ + \text{O}^+ + \text{D}$ via the intermediate $\text{D}^+ + \text{D}^+ + \text{O}$ three-body breakup step [Scenario (1) in Appendix E 1], needs to be considered

as a small contribution, according to our measurement and theoretical description. We begin with the latter.

Out of the three water dication state candidates 2^1A_1 , 1^3A_2 , and 1^1B_1 , only the last state is seen to have a shallow well in symmetric C_{2v} geometry, which supports efficient SOC (see Fig. 13); the other states are purely repulsive. However, a vertical transition from the equilibrium geometry of neutral water produces the 1^1B_1 dication roughly 1 eV above the symmetric barrier near 4.5 bohrs. Furthermore, the isolated crossing between the 1^1B_1 and the 2^3A_2 dication states near 5.5 bohrs is unlikely to result in a charge exchange. Nevertheless, since the 1^1B_1 PEC is steeply repulsive near the equilibrium geometry of neutral water, non-vertical transitions within the FC region can produce dications at or below the aforementioned symmetric barrier that trap dications in the shallow 1^1B_1 potential well and thus increase the probability of a spin-orbit induced charge exchange with the 2^3A_2 state, which we estimate to take over 100 oscillations and, hence, more than 100 femtoseconds. To model this process, we carried out classical trajectory calculations on the 1^1B_1 surface, as was performed in Ref. 20. The idea was to estimate the fraction of the trajectories that pass between the top of the 1^1B_1 barrier at 5.1 eV and the point where the 1^1B_1 and 2^3A_2 surfaces cross, which is 0.25 eV lower, establishing a small appearance window in the potential energy landscape (see Fig. 13 as well as Ref. 49 for a similar appearance window in NH_3).

While sampling from a Wigner distribution of initial states, we selected only those trajectories with a total energy less than 5.1 eV (correlated with the top of the barrier) and having one deuteron with an energy less than 0.25 eV, approximating $\text{KER}_{\text{OD}} \leq 0.25$ eV. Of the 100 000 trajectories sampled leading to the three-body breakup, roughly 0.3% met these criteria, i.e., this small amount of trajectories passes through the narrow energy appearance window where trapping is possible. However, not all such trapped dications must necessarily undergo charge transfer via SOC.

We also found that the accepted trajectories always tend to open the DOD angle, which is also consistent with our finding that,

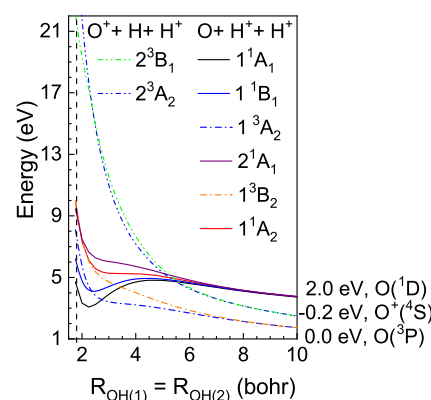


FIG. 13. PECs for the symmetric breakup of the H_2O^{2+} states dissociating into $\text{H}^+ + \text{H}^+ + \text{O}$ and $\text{H}^+ + \text{O}^+ + \text{H}$; adapted from Ref. 20 and corrected by -0.77 eV. The zero energy value of the y-axis corresponds to the $\text{H}^+ + \text{H}^+ + \text{O}(\text{P})$ dissociation limit with a PDI threshold of 36.7 eV.³ The photon energy of 61 eV, hence, corresponds to 24.3 eV on the ordinate.

near the geometry of neutral water, the energy of the 1^1B_1 dication state is lowered with increasing DOD bond angle, i.e., the dissociation angle $\phi_{D^+,D}$ is expected to be bigger than the bond angle of neutral D_2O (104.5°). The small amount of trajectories means that only up to 16% of the 1^1B_1 state contributions in the red rectangle of Fig. 4 fragment in a direct way; the remaining events dissociate sequentially as described in the paper.

We complement the theoretical interpretation with our experimental observations. This is discussed in the lab frame and molecular frame while taking the momentum and angular resolution of the fragments (discussed in Appendix D) into account. The momentum correlation maps of the three heavy fragments in the lab frame are shown in Fig. 14 for the events that reside inside the red rectangle in Fig. 4 and which are associated with the 2^1A_1 , 1^3A_2 , and 1^1B_1 water dication states. Figure 14 reveals that the momentum of the neutral D fragment is ≈ 6 times lower than that of the D^+ ion.

Given this momentum balance, a contribution to the $D^+ + O^+ + D$ fragmentation having low KER_{OD} can be conceivably facilitated via the intermediate $D^+ + D^+ + O$ three-body breakup step [see Fig. 13 and Scenario (1) in Appendix E 1]. We conclude this from the aforementioned non-vertical transitions within the FC region leading to the top of the 1^1B_1 barrier and populating the 2^3A_2 dication surface 0.25 eV below via SOC after a symmetric O–D stretch. During this fragmentation step, the energy of this appearance window is released and mostly distributed equally among the light D^+ ions. Accordingly, both fragments yielded about ≈ 0.125 eV at the crossing (corresponding to a momentum of ≈ 5.8 a.u.), while the oxygen fragment received almost no kinetic energy (≈ 0.025 eV) in this first dissociation step. After the electron transfer, the neutralized D^+ ion is expected to receive no additional energy, which corresponds to the measured momentum of 5.8 a.u. we observe. On the other hand, the O^+ fragment will receive most of its kinetic energy in the subsequent dissociation step between itself and the other D^+ fragment ion. These two ions repel each other due to the Coulomb explosion, and the O^+ ion is emitted in the direction of the neutralized D fragment (we discuss the relative angles in more detail below). Accordingly,

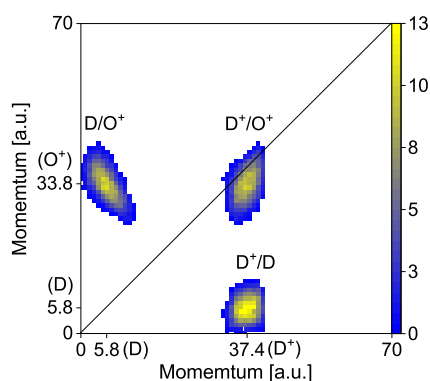


FIG. 14. Lab frame fragment momentum-correlation diagram: yield attributed to the 1^1A_1 and 1^1B_1 dication states of water after PDI at 61 eV resulting in $D^+ + O^+ + D$ for the low KER_{OD} feature, marked as the red rectangle in Fig. 4, as a function of the momenta of the fragment pairs D^+ , O^+ , and D : see labels at axes and islands.

the kinetic energy release KER_{OD} between the O fragment and the to-be-neutralized D^+ ion yields low values that partly reside inside the red rectangle of Fig. 4. After this SOC and state crossing, the 2^3A_2 and 2^3B_1 PECs will lead to the detected final products $D^+ + O^+(^4S) + D$.

Throughout the remaining discussion, we mark the D-fragment subject to electron transfer as D_{II} and the unchanged D^+ ion as D_I^+ for this direct three-body breakup.

After the second step of the dissociation happens and the electron is transferred from the neutral oxygen atom to the deuteron, the neutralized D_{II} fragment no longer experiences a Coulomb repulsion from the other ionic D_I^+ fragment. Instead, the now charged O^+ fragment is repelled by the D_I^+ ion in the third step. Accordingly, the D_I^+ ion is expected to have higher momentum than the O^+ ion, which is corroborated in Fig. 14 (the feature lying just under the diagonal). Furthermore, we expect to see a momentum correlation between the O^+ ion and the neutralized D_{II} fragment, reflecting where, or in other words, how early or late, SOC on the PECs is taking place, as apparent in Fig. 14. The low momentum of the neutral D_{II} fragment and the high momentum of the O^+ ion tell us that the crossing is happening shortly after the direct PDI took place. The crossing would happen later if the momentum of the neutral D_{II} fragment was high and the momentum of the O^+ ion was low. Our momentum map agrees with the former scenario. The momentum map also shows a clear correlation between the neutral D_{II} fragment and the O^+ ion in the sense that the deuteron has less momentum when the O^+ ion exhibits more momentum and vice versa (see the -1 slope of the D/O^+ island in Fig. 14, i.e., the upper left feature). This reflects that the large momentum of the fast D_I^+ fragment is imparted on the $O + D^+$ center of the mass system. Opposite the fast D_I^+ ion, the neutral O fragment appears to follow the slow D_{II}^+ ion, while the latter two particles do not repel each other.

Using the momentum of the neutralized D_{II} fragment in Fig. 14, we can estimate the time between the first and second dissociation steps. Before it is neutralized, the D_{II}^+ ion travels from the FC region at around 1.8 a.u. to the crossing between the 1^1B_1 and 2^3A_2 water dication states at around 5.5 bohrs with a momentum of circa 5.8 a.u. Classically, the time can be estimated at ~ 56 fs.

We support and quantify our findings in momentum space with the analysis of the relative dissociation angles between the measured D_I^+ and O^+ ions and the deduced neutral D_{II} fragment. The relative angle between the O^+ ion and the deuteron presented in Fig. 12 peaked at 40° (blue line). Apparently, both particles were preferentially emitted with a small relative angle, which is necessary for an effective electron transfer between the two fragments in the intermediate step of the dissociation process and which yields low- $KER_{OD_{II}}$. Moreover, we can identify a near back-to-back emission of the O^+ and D_I^+ ions with a relative emission angle peaking at 175° (black line). We also see that the D_I^+ ion and the neutral D_{II} fragment are emitted with a large relative angle, which peaks at 148° (red line) to a degree that is similar to the width of the relative angular distribution between the neutral D_{II} fragment and the O^+ ion. This again points to a larger bond angle of the water dication. A Walsh diagram of the 1^1B_1 dication state of water with an electron in the $4a_1$ orbital shows that, indeed, the bond opening is slightly preferred in the FC region.^{13,20} In summary, the direct three-body fragmentation

scenario [Scenario (1) in Appendix E 1] requires an almost linear water dication in order to produce the $D_1^+ + O^+ + D_{II}$ reaction products. A large relative emission angle between the two D^+ ions was also observed for the direct fragmentation of the 1^1B_1 dication state into $D^+ + D^+ + O$.¹⁴

REFERENCES

- ¹D. Fedorov, S. Koseki, M. W. Schmidt, and M. S. Gordon, "Spin-orbit coupling in molecules: Chemistry beyond the adiabatic approximation," *Int. Rev. Phys. Chem.* **22**, 551 (2003).
- ²C. Marian, "Spin-orbit coupling and intersystem crossing in molecules," *Wiley Interdiscip. Rev.: Comput. Mol. Sci.* **2**, 187 (2012).
- ³P. J. Richardson, J. H. D. Eland, P. G. Fournier, and D. L. Cooper, "Spectrum and decay of the doubly charged water ion," *J. Chem. Phys.* **84**, 3189 (1986).
- ⁴D. Winkoun, G. Dujardin, L. Hellner, and M. J. Besnard, "One- and two-step double photoionisation processes in valence shells of H_2O ," *J. Phys. B: At., Mol. Opt. Phys.* **21**, 1385 (1988).
- ⁵M. N. Piancastelli, A. Hempelmann, F. Heiser, O. Gessner, A. Rüdell, and U. Becker, "Resonant photofragmentation of water at the oxygen K edge by high-resolution ion-yield spectroscopy," *Phys. Rev. A* **59**, 300 (1999).
- ⁶J. Laksman, E. P. Månsson, A. Sankari, D. Céolin, M. Gisselbrecht, and S. L. Sorensen, "Rapid bond rearrangement in core-excited molecular water," *Phys. Chem. Chem. Phys.* **15**, 19322 (2013).
- ⁷G. H. Olivera, C. Caraby, P. Jardin, A. Cassimi, L. Adoui, and B. Gervais, "Multiple ionization in the earlier stages of water radiolysis," *Phys. Med. Biol.* **43**, 2347 (1998).
- ⁸F. Alvarado, R. Hoekstra, and T. Schlathöler, "Dissociation of water molecules upon keV H^+ - and He^{9+} - induced ionization," *J. Phys. B: At., Mol. Opt. Phys.* **38**, 4085 (2005).
- ⁹S. W. J. Scully, J. A. Wyer, V. Senthil, M. B. Shah, and E. C. Montenegro, "Autodissociation of doubly charged water molecules," *Phys. Rev. A* **73**, 040701(R) (2006).
- ¹⁰E. C. Montenegro, S. W. J. Scully, J. A. Wyer, V. Senthil, and M. B. Shah, "Evaporation, fission and auto-dissociation of doubly charged water," *J. Electron Spectrosc. Relat. Phenom.* **155**, 81 (2007).
- ¹¹S. J. King and S. D. Price, "Electron ionization of H_2O ," *Int. J. Mass Spectrom.* **277**, 84 (2008).
- ¹²R. Singh, P. Bhatt, N. Yadav, and R. Shanker, "Kinematics and dissociation dynamics of a water molecule under the impact of 10 keV electrons," *J. Phys. B: At., Mol. Opt. Phys.* **46**, 085203 (2013).
- ¹³B. Gervais, E. Giglio, L. Adoui, A. Cassimi, D. Duflot, and M. E. Galassi, "The H_2O^{2+} potential energy surfaces dissociating into H^+/OH^+ : Theoretical analysis of the isotopic effect," *J. Chem. Phys.* **131**, 024302 (2009).
- ¹⁴D. Reedy, J. B. Williams, B. Gaire, A. Gattón, M. Weller, A. Menssen, T. Bauer, K. Henrichs, P. Burzynski, B. Berry, Z. L. Streeter, J. Sartor, I. Ben-Itzhak, T. Jahnke, R. Dörner, T. Weber, and A. L. Landers, "Dissociation dynamics of the water dication following one-photon double ionization. II. Experiment," *Phys. Rev. A* **98**, 053430 (2018).
- ¹⁵H. C. Straub, B. G. Lindsay, K. A. Smith, and R. F. Stebbings, "Absolute partial cross sections for electron-impact ionization of H_2O and D_2O from threshold to 1000 eV," *J. Chem. Phys.* **108**, 109 (1998).
- ¹⁶A. Hiraya, K. Nobusada, M. Simon, K. Okada, T. Tokushima, Y. Senba, H. Yoshida, K. Kamimori, H. Okumura, Y. Shimizu, A.-L. Thomas, P. Millie, I. Koyano, and K. Ueda, " H_3^+ formation from H_2O^+ mediated by the core-excitation-induced nuclear motion in H_2O ," *Phys. Rev. A* **63**, 042705 (2001).
- ¹⁷I. Ben-Itzhak, A. M. Sayler, M. Leonard, J. W. Maseberg, D. Hathiramani, E. Wells, M. A. Smith, J. Xia, P. Wang, K. D. Carnes, and B. D. Esry, "Bond rearrangement caused by sudden single and multiple ionization of water molecules," *Nucl. Instrum. Methods Phys. Res., Sect. B* **233**, 284 (2005).
- ¹⁸F. A. Rajgara, A. K. Dharmadhikari, D. Mathur, and C. P. Safvan, "Strong fields induce ultrafast rearrangement of H atoms in H_2O ," *J. Chem. Phys.* **130**, 231104 (2009).
- ¹⁹M. Leonard, A. M. Sayler, K. D. Carnes, E. M. Kaufman, E. Wells, R. Cabrera-Trujillo, B. D. Esry, and I. Ben-Itzhak, "Bond rearrangement during Coulomb explosion of water molecules," *Phys. Rev. A* **99**, 012704 (2019).
- ²⁰Z. L. Streeter, F. L. Yip, R. R. Lucchese, B. Gervais, T. N. Rescigno, and C. W. McCurdy, "Dissociation dynamics of the water dication following one-photon double ionization. I. Theory," *Phys. Rev. A* **98**, 053429 (2018).
- ²¹T. Severt, Z. L. Streeter, W. Iskandar, K. A. Larsen, A. Gattón, D. Trabert, B. Jochim, B. Griffin, E. G. Champenois, M. M. Brister, D. Reedy, D. Call, R. Strom, A. L. Landers, R. Dörner, J. B. Williams, D. S. Slaughter, R. R. Lucchese, Th. Weber, C. W. McCurdy, and I. Ben-Itzhak, "Step-by-step state-selective tracking of fragmentation dynamics of water dications by momentum imaging," *Nat. Commun.* **13**, 5146 (2022).
- ²²J. Rajput and C. P. Safvan, "Fragmentation of water by ion impact: Kinetic energy release spectra," *Phys. Rev. A* **84**, 052704 (2011).
- ²³K. H. Tan, C. E. Brion, P. E. Van der Leeuw, and M. J. van der Wiel, "Absolute oscillator strengths (10–60 eV) for the photoabsorption, photoionisation and fragmentation of H_2O ," *Chem. Phys.* **29**, 299 (1978).
- ²⁴J. H. D. Eland, "Double photoionisation spectra of methane, ammonia and water," *Chem. Phys.* **323**, 391 (2006).
- ²⁵Interesting alternatives to the approach presented here are multiple-spawning surface dynamics and non-adiabatic *ab initio* molecular dynamics (AIMD) methods, where electronic energies, gradients, and non-adiabatic coupling matrix elements (NACMEs) are computed on-the-fly [see, e.g., B. F. E. Curchod and T. J. Martinez, *Chem. Rev.* **118**, 3305 (2018), and K. Gope *et al.*, *J. Phys. Chem. Lett.* **11**, 8108 (2020)]. For smaller molecules such as water, non-adiabatic AIMD treatments are very much feasible with the presently available computational tools.
- ²⁶W. Iskandar, T. N. Rescigno, A. E. Orel, K. A. Larsen, B. Griffin, D. Call, V. Davis, B. Jochim, T. Severt, J. B. Williams, I. Ben-Itzhak, D. S. Slaughter, and Th. Weber, "Atomic autoionization in the photo-dissociation of super-excited deuterated water molecules fragmenting into $D^+ + O^+ + D$," *Phys. Chem. Chem. Phys.* **25**, 21562 (2023).
- ²⁷Z. Ali, Y.-D. Chuang, D. Kilcoyne, A. Aguilar, S.-K. Mo, and Z. Hussain, "Upgrade of the beamline 10.0.1 at the advanced light source," *Proc. SPIE* **8502**, 85020P (2012).
- ²⁸R. Dörner, V. Mergel, O. Jagutzki, L. Spielberger, J. Ullrich, R. Moshhammer, and H. Schmidt-Böcking, "Cold target recoil ion momentum spectroscopy: A 'momentum microscope' to view atomic collision dynamics," *Phys. Rep.* **330**, 95 (2000).
- ²⁹J. Ullrich, R. Moshhammer, A. Dorn, R. Dörner, L. P. H. Schmidt, and H. Schmidt-Böcking, "Recoil-ion and electron momentum spectroscopy: Reaction-microscopes," *Rep. Prog. Phys.* **66**, 1463 (2003).
- ³⁰T. Jahnke, T. Weber, T. Osipov, A. Landers, O. Jagutzki, L. P. H. Schmidt, C. L. Cocke, M. H. Prior, H. Schmidt-Böcking, and R. Dörner, "Multicoincidence studies of photo and auger electrons from fixed-in-space molecules using the coltrims technique," *J. Electron Spectrosc. Relat. Phenom.* **141**, 229 (2004).
- ³¹R. Dörner, T. Weber, M. Achler, V. Mergel, L. Spielberger, O. Jagutzki, F. Afaneh, C. L. Cocke, and H. Schmidt-Böcking, "3-D coincident imaging spectroscopy for ions and electrons," in *Imaging in Chemical Dynamics* (Oxford University Press, 2000), Chap. 20, pp. 339–349.
- ³²O. Jagutzki, A. Cerezo, A. Czasch, R. Dörner, M. Hattas, M. Huang, V. Mergel, U. Spillmann, K. Ullmann-Pfleger, T. Weber, H. Schmidt-Böcking, and G. Smith, "Multiple hit readout of a microchannel plate detector with a three-layer delay-line anode," *IEEE Trans. Nucl. Sci.* **49**, 2477 (2002).
- ³³M. Krems, J. Zirbel, M. Thomason, and R. D. DuBois, "Channel electron multiplier and channelplate efficiencies for detecting positive ions," *Rev. Sci. Instrum.* **76**, 093305 (2005).
- ³⁴U. Hechtfisher, J. Levin, M. Lange, L. Knoll, D. Schwalm, R. Wester, A. Wolf, and D. Zajfman, "Near-threshold photodissociation of cool OH^+ to $O + H^+$ and $O^+ + H$," *J. Chem. Phys.* **151**, 044303 (2019).
- ³⁵J. E. Sansonetti and W. C. Martin, "Handbook of basic atomic spectroscopic data," *J. Phys. Chem. Ref. Data* **34**, 1559 (2005).
- ³⁶R. de Vivie, C. M. Marian, and S. D. Peyerimhoff, "Spin-forbidden transitions in the presence of an intersystem crossing: Application to the $b^1\Sigma^+$ state in OH^+ ," *Chem. Phys.* **112**, 349 (1987).
- ³⁷J. Rajput, T. Severt, B. Berry, B. Jochim, P. Feizollah, B. Kaderiya, M. Zohrabi, U. Ablikim, F. Ziaee, P. Kanaka Raju, D. Rolles, A. Rudenko, K. D. Carnes,

- B. D. Esry, and I. Ben-Itzhak, "Native frames: Disentangling sequential from concerted three-body fragmentation," *Phys. Rev. Lett.* **120**, 103001 (2018).
- ³⁸T. Severt, "Imaging light-induced molecular fragmentation dynamics," Ph.D. thesis, Kansas State University, 2021.
- ³⁹D. M. Hirst and M. F. Guest, "An *ab initio* study of the excited states of OH⁺," *Mol. Phys.* **49**, 1461 (1983).
- ⁴⁰D. R. Yarkony, "Spin-forbidden predissociation of the rovibronic levels of OH⁺(c¹Π)," *J. Phys. Chem.* **97**, 111 (1993).
- ⁴¹G. Chambaud, B. Levy, J. M. Launay, P. Millie, E. Roueff, and F. T. Minh, "Charge exchange and fine-structure excitation in O-H⁺ collisions," *J. Phys. B: At. Mol. Phys.* **13**, 4205 (1980).
- ⁴²P. C. Stancil, D. R. Schultz, M. Kimura, J.-P. Gu, G. Hirsch, and R. J. Buenker, "Charge transfer in collisions of O⁺ with H and H⁺ with O," *Astron. Astrophys., Suppl. Ser.* **140**, 225 (1999).
- ⁴³J. A. Spirko, J. T. Mallis, and A. P. Hickman, "Calculation of adiabatic and diabatic ³Σ⁻ states of OH⁺," *J. Phys. B: At., Mol. Opt. Phys.* **33**, 2395 (2000).
- ⁴⁴J. A. Spirko, J. J. Zirbel, and A. P. Hickman, "Quantum mechanical scattering calculations for charge exchange: O + H⁺ ↔ O⁺ + H," *J. Phys. B: At., Mol. Opt. Phys.* **36**, 1645 (2003).
- ⁴⁵F. C. Fehsenfeld and E. E. Ferguson, "Thermal energy reaction rate constants for H⁺ and CO⁺ with O and NO," *J. Chem. Phys.* **56**, 3066 (1972).
- ⁴⁶W. Federer, H. Villinger, F. Howorka, W. Lindinger, P. Tosi, D. Bassi, and E. Ferguson, "Reaction of O⁺, CO⁺, and CH⁺ ions with atomic hydrogen," *Phys. Rev. Lett.* **52**, 2084 (1984).
- ⁴⁷T. N. Rescigno, C. S. Trevisan, A. E. Orel, D. S. Slaughter, H. Adaniya, A. Belkacem, M. Weyland, A. Dorn, and C. W. McCurdy, "Dynamics of dissociative electron attachment to ammonia," *Phys. Rev. A* **93**, 052704 (2016).
- ⁴⁸P. L. Gertitschke and W. Domcke, "Time-dependent wave-packet description of dissociative electron attachment," *Phys. Rev. A* **47**, 1031 (1993).
- ⁴⁹K. A. Larsen, T. N. Rescigno, T. Severt, Z. L. Streever, W. Iskandar, S. Heck, A. Gattton, E. G. Champenois, R. Strom, B. Jochim, D. Reedy, D. Call, R. Moshhammer, R. Dörner, A. L. Landers, J. B. Williams, C. W. McCurdy, R. R. Lucchese, I. Ben-Itzhak, D. S. Slaughter, and T. Weber, "Photoelectron and fragmentation dynamics of the H⁺ + H⁺ dissociative channel in NH₃ following direct single-photon double ionization," *Phys. Rev. Res.* **2**, 043056 (2020).
- ⁵⁰L. Wolniewicz, T. Orlikowski, and G. Staszewska, "¹Σ_u and ¹Π_u states of the hydrogen molecule: Nonadiabatic couplings and vibrational levels," *J. Mol. Spectrosc.* **238**, 118 (2006).